12-1968

A study of the B (3He, p)13C and B (3He, 3He) B reactions

Harold L. Adair

To the Graduate Council:

I am submitting herewith a thesis written by Harold L. Adair entitled "A study of the B (3He, p)13C and B (3He, 3He) B reactions." I have examined the final electronic copy of this thesis for form and content and recommend that it be accepted in partial fulfillment of the requirements for the degree of Master of Science, with a major in Physics.

Robert W. Lide, Major Professor

We have read this thesis and recommend its acceptance:

Accepted for the Council:
Carolyn R. Hodges

Vice Provost and Dean of the Graduate School

(Original signatures are on file with official student records.)

August 7, 1968

To the Graduate Council:

I am submitting herewith a thesis written by Harold L. Adair entitled "A Study of the $^{11}B(^{3}He,p)^{13}C$ and $^{11}B(^{3}He,^{3}He)^{11}B$ Reactions." I recommend that it be accepted for nine quarter hours of credit in partial fulfillment of the requirements for the degree of Master of Science, with a major in Physics.

Robert W. Lide
Major Professor

We have read this thesis and recommend its acceptance:

Harold C. Schweinler

Walter C. Koehler

Jerome L. Duggan

Accepted for the Council:

Hilton A. Smith
Vice Chancellor for
Graduate Studies and Research

A STUDY OF THE $^{11}B(^{3}He,p)^{13}C$ AND $^{11}B(^{3}He,^{3}He)^{11}B$ REACTIONS

A Thesis

Presented to

the Graduate Council of

The University of Tennessee

In Partial Fulfillment

of the Requirements for the Degree

Master of Science

---

by

Harold L. Adair

December 1968

ACKNOWLEDGMENTS

The author wishes to express his appreciation to the Oak Ridge National Laboratory* for the use of the equipment in the experiment. In addition, the author would like to thank the following people: Dr. J. L. Duggan of Oak Ridge Associated Universities under whose direction this research was conducted; Dr. R. W. Lide of the University of Tennessee who served as faculty advisor; Dr. P. D. Miller of the Oak Ridge National Laboratory and Dr. R. L. Dangle of the University of Georgia for their assistance in obtaining the experimental data; Dr. J. Y. Park of North Carolina State University for providing the optical model fits for the elastic scattering data; F. Sluss of the Isotope Target Center of the Oak Ridge National Laboratory for preparing the boron targets used in the experiment; and E. H. Kobisk of the Isotope Target Center for his encouragement during the experiment.

Finally, the author is grateful to Miss Anne Caylor for typing the final manuscript.

*Research sponsored by the United States Atomic Energy Commission under contract with the Union Carbide Corporation.

ABSTRACT

The purpose of this experiment was to study the $^{11}B(^{3}He,p)^{13}C$ and the $^{11}B(^{3}He,^{3}He)^{11}B$ reactions. The proton angular distributions were analyzed in terms of the plane wave stripping theory of Newns and the optical model was used to fit the elastic scattering data.

All the experimental measurements were made with the 5.5 Mev Van de Graaff at the Oak Ridge National Laboratory. The reaction products were observed with silicon surface barrier detectors. A particle identification system, which identifies the type and energy of the incident particle, was used to facilitate the interpretation of the pulse-height spectra.

Proton angular distributions, corresponding to the ground and first excited states of ^{13}C for an incident ^{3}He energy of 12 Mev and for the ground, first, second, sixth, eighth, ninth, and thirteenth excited states of ^{13}C for an incident ^{3}He energy of 10 Mev, were obtained. Spin and parity assignments were made for the eighth and thirteenth excited states of ^{13}C for which no values have been reported. The spin and parity assignments for the other groups were consistent with those reported from other experiments.

The elastic scattering of ^{3}He particles was analyzed at 8, 10, and 12 Mev. The experimental results were satisfactorily interpreted in terms of the optical model.

TABLE OF CONTENTS

LIST OF FIGURES

CHAPTER I

INTRODUCTION

When charged particles are used to bombard target nuclei, a number of reactions can take place (1)*:

1. Elastic Scattering
   a. Coulomb scattering — The electrical charges of the incident particles and the target particles cause the incident particles to be elastically scattered.
   b. Nuclear potential scattering — The incident charged particles pass close to the target nuclei and are elastically scattered by the nuclear forces.
2. Inelastic Scattering
   a. Coulomb excitation — The electric field of the incident particles interacts with the electric moments of the target particles and raises the target particles to higher energy states.

---

*Numbers in parentheses refer to similarly numbered items in the List of References.

b. Surface scattering — The incident charged particle interacts with one or more nucleons at the surface of the target and is scattered inelastically.

3. Surface Transmutation or Knock-Out Reactions

The incident particle ejects one or more particles from the target nucleus.

4. Pickup Reactions

The incident particle picks up one or more nucleons from the target nucleus.

5. Stripping Reactions

The incident particles, composed of two or more subunits, pass near a target nucleus and lose one or more nucleons to the target nucleus.

6. Compound Nucleus Formation

The incident particle reacts with the target nucleus and forms a compound system. The mass number and charge of the compound system are the sum of the mass numbers and charges of its component parts. The nucleons in the compound nucleus are assumed to be bound by strong interactions. As a result, the energy of the nucleons which combine to form the

> compound nucleus is shared among all the nucleons. The decay of the compound nucleus is independent of its mode of formation and can take place in a number of ways subject only to its degree of excitation (2).

The study of a nuclear reaction yields information about nuclear structure and about specific properties of the nuclear states formed in a given reaction (3). At present the many-body problem which a nuclear reaction poses cannot be solved. Thus, to analyze a nuclear reaction, one has to use a model which approximates the actual situation. In 1936, Bohr proposed one of the first models when he pointed out that it was useful to divide a nuclear reaction into two states: (1) the formation of a compound system, and (2) the disintegration of the compound system into the products of the reaction (4). As indicated previously, the mode of disintegration of the compound nucleus depends only on its energy, angular momentum, and parity and is independent of the way in which it was formed. The compound nucleus model has been successful in explaining many features of nuclear reactions; the most important are the resonances in the yield curves and the symmetry of the angular distributions about 90° (5).

The compound nucleus model has not been successful in explaining a number of nuclear reactions. To explain these reactions, a direct interaction model was postulated. In the direct interaction model, the incident particle reacts directly with a nucleon near the surface of the target nucleus. If one assumes a mean free path of the order of

nuclear dimension, the incident particle can react without the formation of a compound nucleus (6). All those reactions discussed earlier, except the compound nucleus formation, are classified as direct interaction processes.

Some of the general features of the direct interaction processes are (7):

1. The energy spectrum of the emitted particles is different from the Maxwellian form obtained from the compound nucleus model. In the direct interaction model, there is a higher probability of exciting low-lying states in the residual nucleus.
2. There is a high probability of emitting the same type particle as that striking the target nucleus. The compound nucleus favors the emission of neutrons.
3. The angular distributions tend to be peaked at the forward or backward angles and are not symmetric about 90°.

In the direct interaction processes, it is assumed that the direct interaction is confined to the surface of the target nucleus (6). If one assumes that a nucleon "a" bombards a target nucleus composed of a core C and an extracore particle b, the direct interaction processes can be illustrated as follows (8):

1. Elastic Scattering

$$a + (b + C) \longrightarrow a + (b + C)$$

2. Inelastic Scattering

$$a + (b + C) \longrightarrow a + (b + C)^{*}$$

3. Surface Transmutation or Knock-Out Reaction

$$a + (b + C) \longrightarrow (a + C) + b$$

4. Pickup Reaction

$$a + (b + C) \longrightarrow C + (a + b) \ .$$

If the incident particle is composed of two or more subunits, as in deuteron or ^{3}He stripping reactions, ordinary or exchange stripping can occur when one subunit of the incident particle is stripped or exchanged with the extracore particle. Double or triple stripping occurs when two or three subunits are stripped from the incident particle:

5. Ordinary Stripping

$$(a_1 + a_2) + (b + C) \longrightarrow a_1 + (a_2 + b + C)$$

6. Exchange Stripping

$$(a_1 + a_2) + (b + C) \longrightarrow (a_1 + b) + (a_2 + C) \ .$$

Stripping reactions are very useful in the study of nuclei because the stripping cross sections as functions of angle and energy are very dependent on the spins and parities of the nuclear levels involved. If the spin and parity of the ground state of the target nucleus are known, spin and parity assignments can be made to the appropriate level in the residual nucleus (9).

---

*The target is left in an excited state.

The most suitable projectile for stripping is the deuteron. Since the proton and neutron are weakly bound with a binding energy of 2.23 Mev and have a fairly large average distance of separation, the proton or neutron can be captured by a target nucleus and the remaining nucleon passes by the target nucleus and interacts very weakly with it (10). The resulting reactions are of the form (d,p) or (d,n).

The success of Butler's direct interaction theory in fitting experimental data from deuteron-induced reactions prompted the study of more complicated reactions to see if these reactions proceeded by a direct process. It was thought that ^{3}He reactions such as (^{3}He,d) which involved the transfer of a single nucleon might be subject to a similar analysis.

In addition to single particle stripping, there was considerable interest in those reactions which involved the transfer of two or more nucleons such as the (^{3}He,p), (t,p), (d,α), (α,d), and (α,p) reactions. The theoretical treatment of nuclear reactions which involve the stripping of two or more nucleons has been very limited. Tobocman and Butler considered the case of several nucleons being transferred from the projectile to the target nucleus (11 and 12). In this treatment the stripped particles were considered to have no structure. The projectile was treated as two lumps of nuclear matter bound together. One lump of the nuclear matter would be stripped off and captured by the target nucleus and the other would emerge. The structure of the projectile and the stripped nucleus are included in the two nucleon stripping formulas of Newns and el Nadi (13 and 14). Since the

publication of the two nuclear stripping theories by Newns and by el Nadi, it has become evident that a large number of reactions of the type (^{3}He, p) could be successfully described in terms of this model.

An advantage of using ^{3}He as a projectile in the study of nuclear reactions is its high mass excess, 15.814 Mev, which leads to high positive Q values (15). The high Q values associated with ^{3}He reactions make possible the detailed study of the deexcitation of states in final nuclei at high excitations even at low incident energies.

The (^{3}He, p) reaction has been investigated over a range of incident energies by a number of groups (16 through 25). Most of the reported work has been done at energies between $0.8 \leq E(^3He) \leq 10$ Mev. At present the experimental information available for ^{3}He-induced reactions is not as easy to interpret as that for the deuteron reactions. For this reason, the use of ^{3}He-induced reactions as spectroscopic tools for the determination of level parameters is sometimes difficult. Although the stripping mechanism does not satisfactorily explain the angular distribution for ^{3}He-induced reactions for all projectile energies, it appears to be the dominant process for incident energies in the range of 5 to ~15 Mev (26).

Angular distributions for proton groups from the $^{11}B(^3He, p)^{13}C$ reaction have been measured at incident ^{3}He energies of 0.900, 1.25, 3.0, 3.50, 4.5, 4.9, 5.4, 6.05, 8.6, 9.6, and 10.3 Mev (27 through 31). At 4.5 and 5.4 Mev, Holmgren, Wolicki, and Johnston observed seven proton groups, a number of which showed forward peaking. A yield curve for three proton groups was obtained over the energy range of 3.00 to 5.40

Mev. They concluded that the angular distributions and yield curves for the proton groups could not be accounted for on the basis of forward stripping and that some other process was involved. However, they further stated that their data were not inconsistent with the trend for low Q (^{3}He, p) reactions to behave like compound nucleus reactions and high Q reactions like direct interactions. The angular distribution for the ground state proton was measured at 8.6, 9.6, and 10.3 Mev by Marsh and Bilaniuk. Also, differential excitation functions were measured in 200-kev intervals from 8.0 to 11.0 Mev for a θ_L of 35° and 140°. The forward peaking of the angular distribution of the ground state proton group and the absence of sharp resonances in the yield curves indicated that the reaction proceeds mainly by a direct process.

Angular distributions of protons from the $^{10}B(\alpha, p)^{13}C$ reaction have been investigated at alpha energies of 4.9, 7.0, 8.1, 12.1, 13.4, 14.7, 16.0, 20.6, 21.4, 22.2, 27.5, 30.4, 33.0, and 33.1 Mev (32 through 36). The angular distributions obtained at different energies show strong variations with energy; however, the presence of a diffractional character in these angular distributions indicates that the predominant mechanism is direct interaction (37).

A number of ^{3}He reactions have been analyzed in terms of the distorted wave theory (38 and 39). In contrast to the plane wave theory, the distorted wave theory takes into account the distortion of the incident and scattered wave by the nuclear potential. To apply distorted wave calculations, it is helpful to know the distorting

potentials, which can be obtained through an optical model analysis of elastic scattering discussed in Chapter II, pages 12 through 15.

The elastic scattering of neutrons, protons, deuterons, and alpha particles has been successfully analyzed over a wide range of energies in terms of the optical model (40 through 45). In general, very little data for the optical model treatment of the elastic scattering of ^{3}He particles are available. However, the elastic scattering of ^{3}He particles by both light and medium weight nuclei has been investigated at a few incident energies (46 through 50). In most cases the resulting experimental data have been analyzed in terms of the optical model and have given good agreement with the elastic scattering cross sections (51 and 52).

The purpose of this experiment was to look at some of the excited states of ^{13}C in the $^{11}B(^{3}He,p)^{13}C$ reaction at bombarding energies of 10 and 12 Mev and to look at the elastic scattering of ^{3}He by ^{11}B at 8, 10, and 12 Mev. Previous data for ^{3}He-induced reactions were obtained at relatively low bombarding energies where the Coulomb effects are important. The higher bombarding energies may give a clearer understanding of the ^{3}He-induced reactions and provide spectroscopic information for the determination of level parameters (53). The elastic scattering data were analyzed in terms of the optical model.

CHAPTER II

DISCUSSION OF EQUATIONS USED FOR THEORETICAL ANALYSIS OF DATA

I. DOUBLE STRIPPING ANALYSIS

If a projectile whose nucleons are weakly bound is incident on a target, it is possible for one or more of the projectile nucleons to be captured by the target nucleus. The remainder of the incident nucleons react very little with the target and the residual nucleus and are emitted. This process is called a stripping reaction.

Butler indicated that stripping reactions could possibly be used to study nuclear properties (54). This conclusion was supported by the fact that there are certain restrictions on the orbital angular momentum of the stripped nucleons which must be met before the nucleons can be captured by the target nucleus. That is, the orbital angular momentum of the absorbed nucleon and its spin and the initial nuclear spin of the target must correspond to the spin of the level in which the residual nucleus is formed (55). If $\vec{J}_o$ and $\vec{J}_f$ are the initial and final nuclear spins and $\vec{S}$ is the spin of the captured nucleons, the vector coupling rule states that

$$\vec{J}_f = \vec{J}_o + \vec{L} + \vec{S} \quad , \tag{1}$$

where $\vec{L}$ is the orbital angular momentum of the captured nucleons. The orbital angular momentum of the captured nucleons is further restricted by the conservation of parity. If the levels of the initial and

residual nuclei have the same parity, $\vec{L}$ is even. If the relative parity of the levels of the initial and residual nuclei is odd, $\vec{L}$ is odd.

Butler indicated through a semiclassical argument how the orbital angular momentum, $\vec{L}$, of the absorbed nucleons determines the stripping angular distribution (56). If the momentum of the incident and emitted particle is given by $\vec{K}_i$ and $\vec{K}_e$, respectively, the momentum $\vec{K}_c$ carried into the target nucleus is

$$\vec{K}_c = \vec{K}_i - \vec{K}_e \quad , \tag{2}$$

where $\vec{K}_c$ is a function of the angle between $\vec{K}_i$ and $\vec{K}_e$ and is smallest when the angle is equal to 0. Thus, the maximum orbital angular momentum carried into the target nucleus by the stripped nucleon or nucleons is given by $\vec{K}_c r_o$ where r_o is the radius of the initial nucleus. As shown in Equation (1), the condition $\vec{K}_c r_o \geq \vec{L}$ must exist for the reaction to take place. For $\vec{L} = 0$ all values of $\vec{K}_c$ satisfy the above condition. For this case, the nucleons of the incident projectile tend to split in such a way that the direction of $\vec{K}_e$ is close to that of the incident projectile.

For $\vec{L} > 0$, the orbital angular momentum carried by the stripped nucleons into the target nucleus must usually be equal to $\vec{L}$ before the reaction can proceed. This condition is usually not met for small scattering angles. The stripping angular distributions are a maximum at the angles for which $\vec{K}_c r_o = \vec{L}$.

A theoretical investigation of a double stripping process was made by Newns (13). One limiting approximation in this investigation was to assume the stripped particles have no structure. The projectile

is treated as two lumps of nuclear matter one of which is stripped off and captured by the target nucleus and the other emerges. With this approximation, the differential cross section is given by

$$\sigma(\theta) = \sum_{L} A_L \left| j_L(Kr_o) \right|^2 , \qquad (3)$$

where A_L is the relative intensity of a transition of a definite L value and $j_L(Kr_o)$ is a spherical Bessel function of order L. The orbital angular momentum L imparted to the target nucleus by the captured nucleons is

$$\vec{L} = \vec{l}_n + \vec{l}_p , \qquad (4)$$

where $\vec{l}_n$ and $\vec{l}_p$ are the orbital angular momenta of the captured neutron and proton. The term r_o is the reaction radius and is approximately equal to the nuclear radius. The transferred momentum wave number, $\vec{K}$, for a (^{3}He,p) reaction is given by Newns as

$$\vec{K} = \vec{K}_3 - \frac{M_i}{M_f} \vec{K}_p , \qquad (5)$$

where M_i and M_f are the masses of the initial and final nuclei. The terms $\vec{K}_3$ and $\vec{K}_p$ are the momentum wave numbers of the ^{3}He particle and the emitted proton, respectively (13).

II. OPTICAL MODEL ANALYSIS OF ELASTIC SCATTERING

Inadequacies in existing nuclear models in accounting for the elastic and inelastic scattering of nucleons led to the formulation of the optical model. According to this model, the interaction potential

is composed of a real part, which accounts for the scattering, and an imaginary part, which accounts for absorption.

Prior to the formulation of the optical model, most nuclear reactions were described by the compound nucleus model of Bohr. However, the application of the compound nucleus model for nuclear widths which approached the separation of levels in the compound system proved awkward. It was suggested that a single particle potential function could be used to approximate the results obtained by averaging over the properties of the individual states (57). In 1940, Bethe suggested that the potential should contain an imaginary part to account for the inelastic processes which occur. At that time, the nucleus was considered to be almost entirely opaque to the incoming nucleons. In 1947, Serber suggested that the nucleus might be partially transparent to incident nucleons and concluded that the mean free path for the absorption of high energy nucleons was of the order of nuclear dimensions (58).

In 1952, LeLevier and Saxon used the optical model to successfully correlate the scattering of 20-Mev protons by a complex square-well potential (59). In 1953 and 1954, Feshbach, Porter, and Weisskopf used the optical model in the interpretation of low energy neutron scattering (60). In the latter case, a complex spherical square-well potential was used. The real part of the potential was given a value of ~40 Mev, and the imaginary part was given a very small value. In 1954, proton scattering experiments led Chase et al. to suggest that the square well should be replaced by a diffuse-surface region (61 and 62).

The optical model replaces all the separate interactions between incident nucleons and target nuclei with a two-body interaction. The potential for this interaction has the form (63)

$$U(r) = -\left[VF_R(r) + iWF_I(r) \right] + V_c(r) + V_{so}(r) \quad , \tag{6}$$

where $F_R(r)$ and $F_I(r)$ are functions which give the radial variation of the real and imaginary parts of the complex central nuclear potential. The term $V_c(r)$ is the Coulomb potential and is taken as that potential due to a uniformly charged sphere. If the radius of the charged sphere is $r_c A^{1/3}$, the Coulomb potential is given as

$$V_c(r) = \frac{Z_I Z_T e^2}{2r_c A^{1/3}} \left(3 - \frac{r^2}{(r_c A^{1/3})^2} \right) \text{ for } r \leq r_c A^{1/3} \tag{7}$$

and

$$V_c(r) = \frac{Z_I Z_T e^2}{r} \text{ for } r > r_c A^{1/3} \quad . \tag{8}$$

For $F_R(r)$, the radial variation of the real part of the complex central nuclear potential, the Saxon-Woods form factor $f(r)$ is used,

$$f(r) = \left[1 + \exp\left(\frac{r - r_o A^{1/3}}{a} \right) \right]^{-1} \quad , \tag{9}$$

where $r_o A^{1/3}$ is the nuclear radius, and "a" is the diffuseness of the nuclear surface. For the imaginary part $F_I(r)$, two different forms can be used to obtain the best fit to the experimental values. One is the Saxon-Woods volume absorption,

$$F_I(r) = f(r) \quad . \tag{10}$$

The other is the Gaussian surface absorption

$$F_I(R) = g(r) = \exp\left[- \left(\frac{r - r_{o_g} A^{1/3}}{b} \right)^2 \right] , \qquad (11)$$

where b is equal to the width of the Gaussian and r_{o_g} is the nuclear Gaussian radius constant. The term V_{so} is the spin-orbit potential and is taken to be of the Thomas form

$$V_{so}(r) = - \left(\frac{\hbar}{2 MC} \right)^2 (V_s + iW_s) \frac{1}{r} \frac{d f(r)}{dr} (\vec{\sigma} \cdot \vec{l}) . \qquad (12)$$

The computations were carried out by J. Y. Park at North Carolina State University using a least-squares fitting program SKAT12. The variable parameters were systematically varied to find the minimum value of the quantity X^2 defined by

$$X^2 = \frac{1}{N} \sum_{i=1}^{N} \left[\frac{\sigma_{th}(\theta_i) - \sigma_{exp}(\theta_i)}{\Delta\sigma_{exp}(\theta_i)} \right]^2 , \qquad (13)$$

where the summation is carried out over all the experimental points. The terms $\sigma_{th}(\theta_i)$ and $\sigma_{exp}(\theta_i)$ are the calculated and experimental cross sections, respectively, at angle θ_i, and $\Delta\sigma_{exp}(\theta_i)$ is the experimental error (64). Buck, Maddison, and Hodgson (64) describe how the Schrödinger wave equation can be used to calculate the observable cross sections for two particles interacting through the potential given in Equation (6).

CHAPTER III

EXPERIMENTAL PROCEDURE

I. PREPARATION OF BORON TARGETS

Many techniques are described in the literature for preparing self-supporting films of boron (65 through 71). These include vapor plating, painting with boron from an oil suspension, and vacuum evaporation. As summarized by Muggleton and Howe (65), techniques other than evaporation-condensation and vapor plating usually yield thick nonuniform films of boron which have inferior chemical purity and are unsuitable for nuclear spectroscopy experiments. Uniform films can be produced by vapor plating but the procedure is hazardous. Vacuum evaporation by resistance heating has been used to evaporate boron from a graphite crucible (67), but the evaporation rate is slow and the resulting film is usually contaminated by crucible material.

Vacuum evaporation by electron bombardment heating was the method selected to produce the boron films for the studies in this report. By using this method of heating, the evaporation temperature, ~2300° C, can be attained quite rapidly after the boron has been thoroughly outgassed. Contamination by crucible material is eliminated because the boron being evaporated serves as its own crucible. A boron pellet before and after evaporation is shown in Figure 1.

The electron bombardment furnace used for evaporation is shown in Figure 2. The furnace is composed of stainless steel components and

Figure 1

Boron Pellet Before and After Electron Bombardment

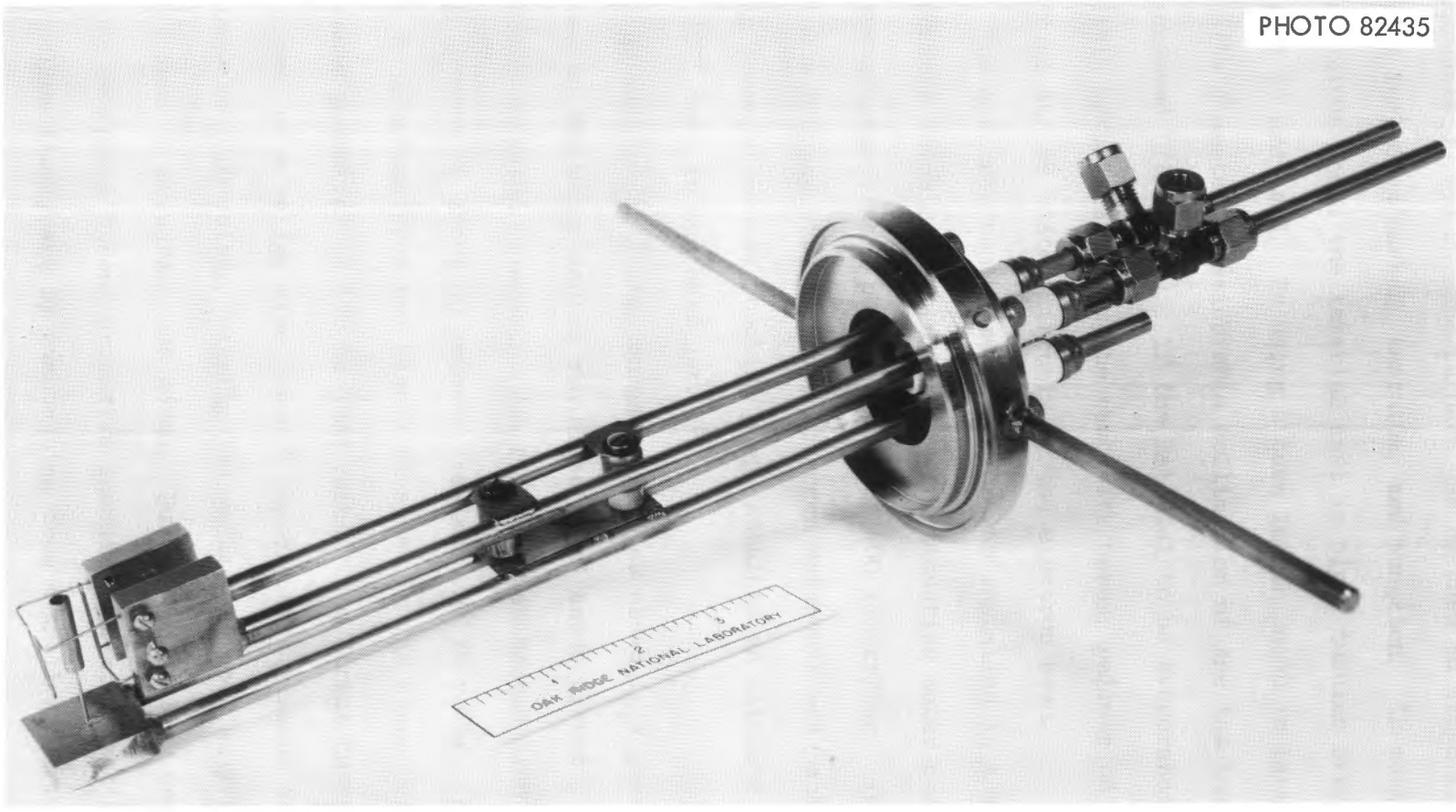

Figure 2

Electron Bombardment Furnace

is bakeable to 450° C. The furnace can be used to evaporate most materials including carbon, tantalum, and tungsten. In most isotopic evaporations where the material cost is high, tubular crucibles (Figure 3) are used. By using a tube length which is large compared with its diameter, considerable collimation of the issuing vapors can be achieved (72 and 73). If the material to be evaporated reacts with crucible materials, as is the case with boron, pellets or bars of the material can be heated directly by the electron beam.

The electron bombardment furnace was installed in a Veeco vacuum evaporator which contained a 4-in. fractionating water-cooled oil diffusion pump with a pumping speed of 400 liters/sec. The pump, when suitably trapped with a liquid nitrogen reservoir and backed by a 5 cubic feet per minute roughing pump, attained an ultimate vacuum of 2×10^{-7} torr in the bell jar.

A cylindrical 2-gram boron pellet, as shown in Figure 1, was placed on the water-cooled stainless steel anode directly below a circular tungsten filament. The filament was heated with an alternating current of about 50 amperes (maximum) at 10 volts. Electrons were accelerated from the heated filament to the boron pellet by a variable potential of 100 to 1000 volts. The direct current supply consisted of a bridge type circuit capable of a maximum output of 3 amperes at 1000 volts. Usually 500 watts generated at 1 kilovolt was sufficient to evaporate the boron. During the heating and evaporation of the amorphous boron, excessive sparking was minimized by heating the pellet slowly and by evaporating from a small section in the center

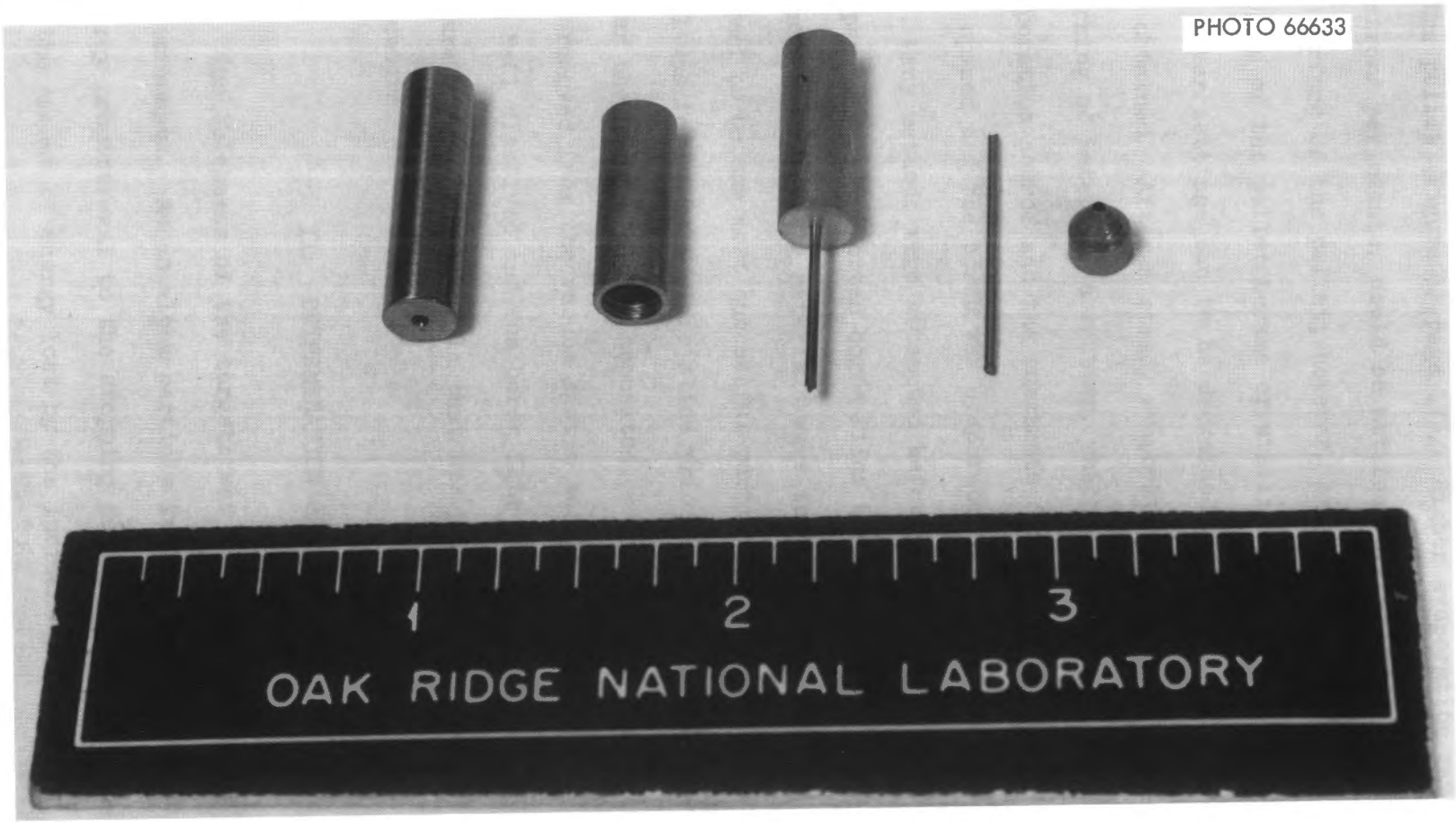

Figure 3

Tubular Crucibles

of the pellet (Figure 1, page 17). Higher evaporation rates, ~300 angstroms per minute, could be attained by uniformly heating the entire top surface of the pellet; however, excessive sparking occurred, and the top of the pellet became crystalline and had a mushroom appearance. The power settings had to be decreased until a steady evaporation rate was obtained. After a steady evaporation rate was obtained with no sparking of material, a shutter, which had been placed between the evaporation source and the substrate during the initial outgassing, was opened and the boron was evaporated.

Many methods were attempted before a satisfactory procedure for preparing self-supported boron films was obtained. Several parting agents and substrate materials were investigated. Sodium chloride proved to be the most successful parting agent used. A thin film of NaCl was formed on a glass slide prior to the evaporation of boron. After the boron had been deposited on the NaCl surface, the glass slide was removed from the vacuum system and slowly immersed in a water bath. The NaCl dissolved and the boron film floated on the water surface. Figure 4 shows a boron film that was prepared by the previous described procedure.

II. DETERMINATION OF TARGET THICKNESS

The thickness of the targets was determined by alpha thickness measurements. As an alpha particle travels through the film, it loses energy proportional to the stopping power of the film, which is defined as the amount of energy lost by the incident particle per centimeter

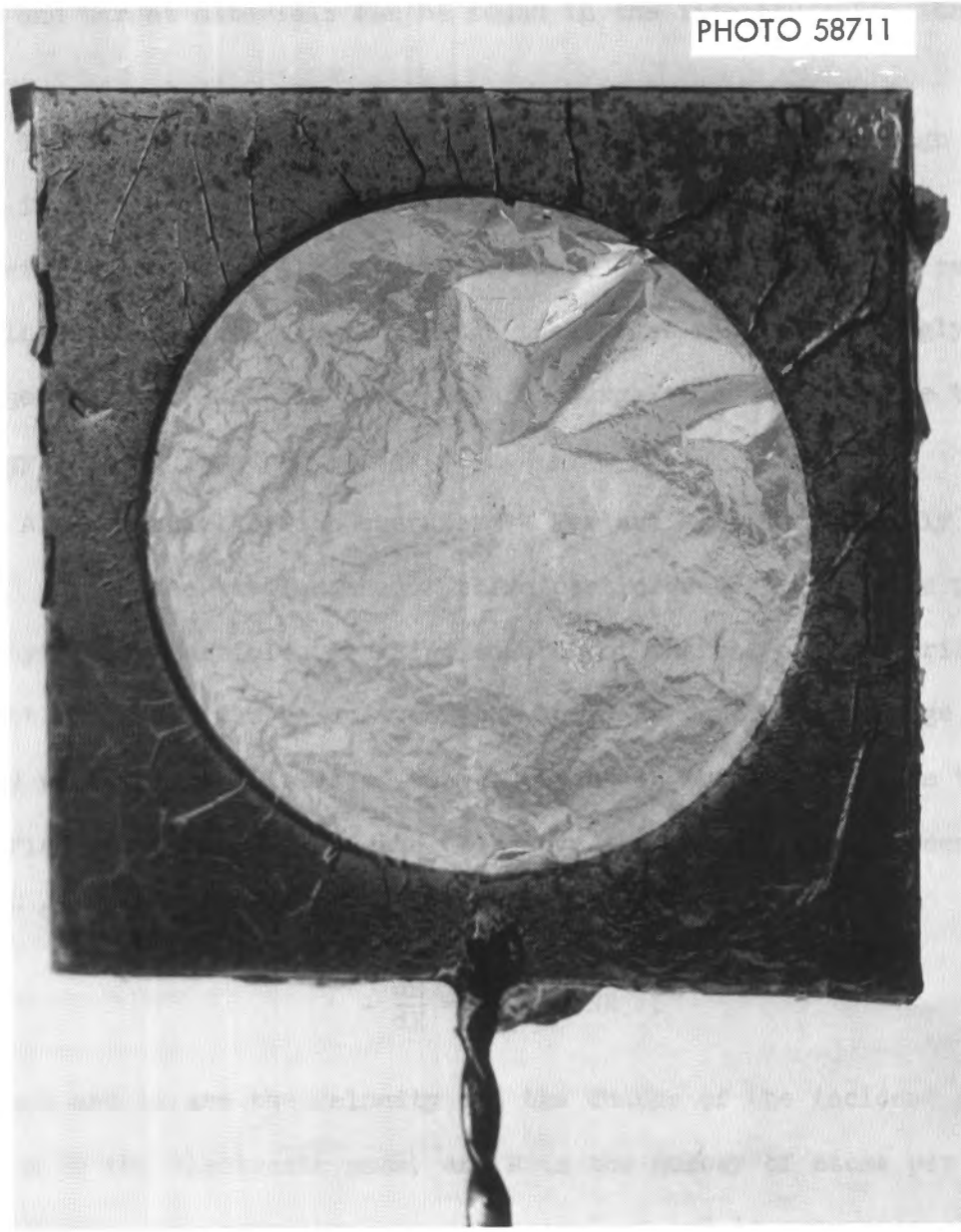

Figure 4

Self-Supporting Boron Film

of target thickness. Stopping power data for numerous incident particles and target materials can be found in the literature (74 through 80).

The energy lost by an alpha particle as it travels through the film is mainly due to ionization and excitation of the atoms in the material traversed. Alpha particles with an energy of <1 Mev can pick up electrons as they travel through the target and become singly charged or neutral. The reduction in charge tends to decrease the energy loss of slow particles (74).

Alpha particles with energies >4 Mev are almost completely ionized. Since the wavelengths of these particles are short, the probability of the particles exciting an atom of the stopping material is slight (75). If the velocity of the incident particle is large compared with the velocities of the electrons in the atoms of the target material, Livingston and Bethe (74) give the energy loss per centimeter of path as

$$-\frac{dE}{dX} = \frac{4\pi e^4 z^2}{mv^2} NB \quad , \tag{14}$$

where v and ez are the velocity and the charge of the incident particle, m is the electronic mass, and N is the number of atoms per cubic centimeter. The quantity B is dimensionless and is proportional to the stopping power. For a particle so energetic that its trajectory is almost a straight line, B can be written as (74 and 75)

$$B(Z,v) = Z \ln\left(\frac{2mv^2}{I}\right) \quad , \tag{15}$$

where Z is the atomic number of the stopping material and I is defined as the average excitation potential of the atom. For relativistic particles, the quantity B is written as (74)

$$B = Z \ln \left(\frac{2mv^2}{I}\right) - \ln (1 - \beta^2) - \beta^2$$

$$B = Z \ln \frac{2mv^2}{I(1 - \beta^2)} - \beta^2 \quad , \tag{16}$$

where β = velocity of incident particle/velocity of light = v/c. After substitution, Equation (14) becomes

$$-\frac{dE}{dX} = \frac{2\pi e^4 z^2}{mv^2} NZ \left[2 \ln \frac{2mv^2}{I(1 - \beta^2)} - 2\beta^2 \right] , \tag{17}$$

$$-\frac{dE}{dX} = \frac{2\pi e^4 z^2}{m\beta^2 c^2} NZ \left[\ln \frac{(2mv^2)(2mv^2)}{I^2(1 - \beta^2)} - 2\beta^2 \right] . \tag{18}$$

The maximum energy transfer to an electron from an incident particle is given by Livingston and Bethe (74) as

$$Q_{max} = 2mv^2 \quad . \tag{19}$$

By substituting in Equation (18) the following can be written:

$$-\frac{dE}{dX} = \frac{2\pi e^4 z^2}{m\beta^2 c^2} NZ \left[\ln \frac{2m\beta^2 c^2 Q_{max}}{I^2(I - \beta^2)} - 2\beta^2 \right] . \tag{20}$$

According to Livingston and Bethe, Equation (20) is applicable to alpha particles with energies of >1 Mev (75). A correction to the equation for lower particle velocities is given in Reference 79.

The alpha emitter selected for the source was ^{241}Am. The main alpha group has an energy of 5.477 Mev. The energy (5.435 Mev) of a

second group with ~15 percent of the intensity does not interfere with measurements of the main group. A silicon p-n junction diode was used as the alpha detector. The output from the detector was amplified and fed into a 1024-channel pulse-height analyzer. The resolution of the system with no foil in place was 15 kev. When a boron film was inserted, the resolution decreased due to alpha straggling through the film. The boron film was mounted between the ^{241}Am source and the detector in a vacuum chamber. A typical pulse-height spectrum showing the shift in peak position obtained when the film is in place is shown in Figure 5. The stopping power data used in the thickness measurements was taken from Reference 79. The accuracy of the data is stated to be ±10 percent. The error in the energy loss measurements is within ±5 percent which indicates that the actual foil thickness may vary as much as ±15 percent.

III. SEMICONDUCTOR PARTICLE DETECTORS

Semiconductor crystals have been used as detectors since 1945 (81). When a high energy charged particle is incident on a crystal, it will interact with bound electrons in the material and produce hole-electron pairs along its path. Since semiconductor materials have a band gap of approximately 1 ev between the conduction and the valence band, an electric field can be maintained across the material without producing large currents. The applied field allows the holes and electrons formed by an incident particle to be swept out of the crystal to conducting electrodes. However, for most semiconductor materials at

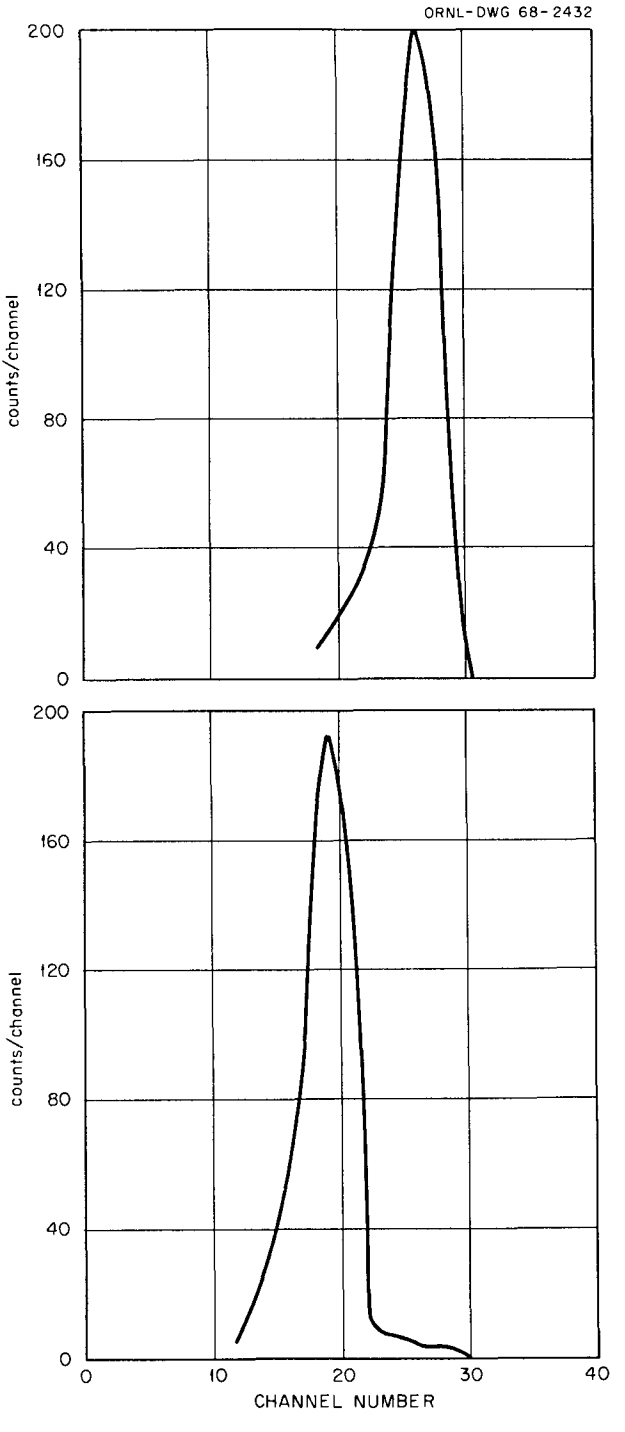

Figure 5

Pulse-Height Spectrum Showing Shift in Peak Position Due to Alpha Energy Loss in Boron Film

room temperature, the number of hole-electron pairs produced by an incident particle is small compared with the number of free hole-electron pairs that exist in the material. The presence of the free hole-electron pairs is caused by an electron in the filled valence band which is thermally excited and raised to the conduction band (82 and 83). For example, silicon, which has a band gap of 1.2 volts, contains $\sim 10^{10}$ free hole-electron pairs per cubic centimeter (82).

To use semiconductor materials as detectors, the number of free hole-electron pairs is reduced by making use of the properties of a p-n junction. At the junction between p- and n-type material a small region (the depletion region) exists where no carriers exist. This region can be enlarged by applying an electric field in the appropriate direction (82 and 83). Thus, if n-type material is introduced into one section of a semiconductor crystal, and p-type material is introduced into the remainder of the crystal, a p-n junction can be formed. The section of the crystal doped with n-type material contains an excess of electrons, and the section doped with p-type material contains an excess of holes. By applying an electric field across the crystal from the n-type material toward the p-type material (reverse bias), a depletion region is formed.

A charged particle incident on the depleted region will interact with bound electrons in the material and raise them from the valence band; thereby, hole-electron pairs are created. The energies required to form an electron-hole pair in silicon and germanium are 3.6 and 2.9 ev, respectively (84).

The hole-electron pairs will be removed from the depleted region to conducting electrodes by the electric field. The electric field must be strong enough to remove the hole-electron pairs before any recombination can occur. The resulting pulse produced in an external circuit will be proportional to the energy of the incident particle, if all the energy of the particle is lost in the depleted region.

The reaction products in this experiment were observed with silicon surface barrier detectors. The detectors were fabricated by Oak Ridge Technical Enterprises Corporation (ORTEC) by forming a thin p-type layer on the surface of n-type silicon by oxidation. Electrical contact was made to the p-type surface through a thin gold film $\sim$40 micrograms/cm^2. A nonrectifying metal contact was used for the n-type silicon (84).

A resolution of 15-20 kev is not uncommon for silicon semiconductor detectors. However, better resolution can be obtained by cooling the detectors. Cooling reduces the noise in the detector due to leakage current. When the detector is cooled, the leakage current decreases by a factor of $\sim$3 for every 10°C, and the noise level decreases by $\sim \sqrt{3}$ for every 10°C. This levels out at about 50°C below zero (85).

The detectors used in this experiment were cooled with trichloroethylene which was circulated through dry ice. The electronic resolution of the system, obtained by using a pulser, was $\sim$20 kev. The resolution for protons was 50 kev. This was sufficient for the nuclear levels studied in this experiment.

IV. ELECTRONICS

One of the problems involved in the study of nuclear structure with accelerators is the interpretation of the complex spectra that are obtained. Since the final nucleus can exist in any one of several excited states, the energy of the outgoing particle can cover a wide range. Thus, data interpretation could be simplified by a particle identification system that would identify the type of particle emitted and the energy of the particle.

As a particle travels through matter, it loses energy. The energy loss as a function of distance through the material varies for different particles. Many measurements of these dE/dX values for various particles have been made (74 through 80). This differential energy loss principle is used as the basis for the particle identifier.

Two semiconductor detectors were used to measure the energy of the charged particles of interest. The two detectors were aligned so that a particle passed through and lost a finite amount of energy in the transmission-mounted detector, ΔE, and was totally absorbed in the E detector (Figure 6).

For incident particle energies E_T of the order $10 \leq E_T \leq 100$ Mev, the range and incident particle energy are related by the empirical relationship

$$R = AE_T^{1.73} \quad , \tag{21}$$

where A is a constant that depends on the type of particle (86 and 87):

$$A \simeq \frac{1}{M^{0.73}Z^2} \quad . \tag{22}$$

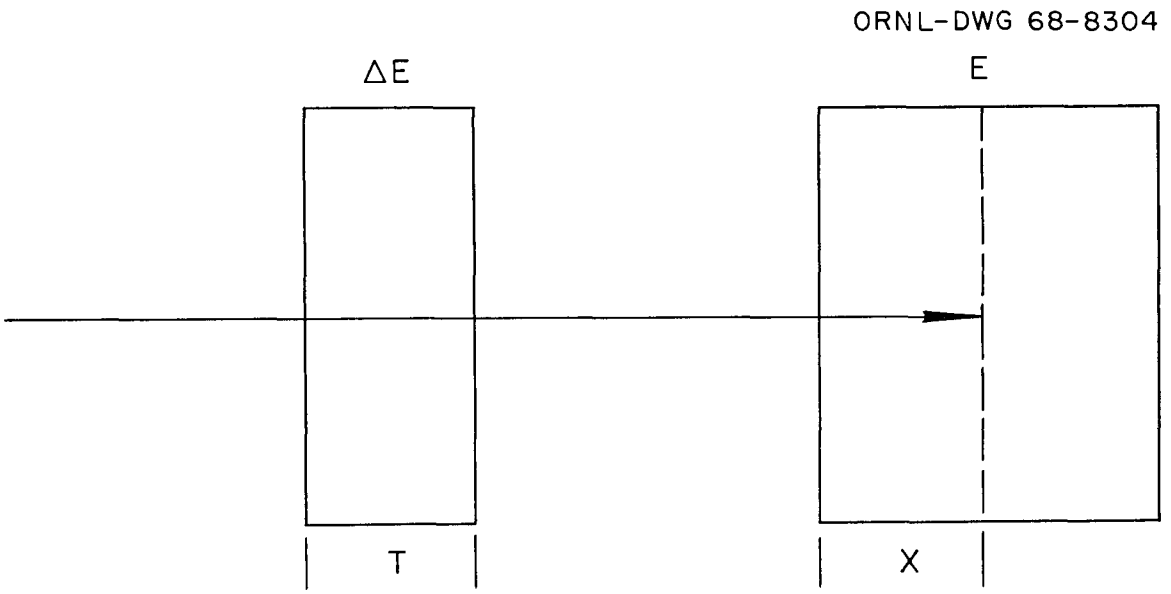

Figure 6

Diagram Showing a Particle Penetrating ΔE Detector and Being Stopped in E Detector

From Figure 6 and Equation (21), the following can be written:

$$(T + X) = A(E + \Delta E)^{1.73} \quad . \tag{23}$$

For the E detector,

$$X = AE^{1.73} \quad . \tag{24}$$

From Equations (23) and (24), the quantity T/A can be written as

$$T/A = (E + \Delta E)^{1.73} - E^{1.73} \quad . \tag{25}$$

The ratio T/A is characteristic of the particle that penetrates the ΔE detector and stops in the E detector.

A schematic of the particle identification electronics is shown in Figure 7. The signals from the ΔE and E detectors are fed through preamplifiers and main amplifiers to a coincidence circuit. Only those signals which enter ΔE and E in coincidence are allowed to enter the particle identifier. From the coincidence circuit the signals travel through pulse stretchers to provide an input pulse of ~4 microseconds for the particle identifier.

The signals arriving at the particle identifier in coincidence are allowed to enter the gated sum where they are added linearly. The E signal passes through the gated sum unchanged for 1.8 microseconds and then the ΔE signal is added to the E signal for 1.8 microseconds. The coincidence circuit provides the start signal for the timing generator. The timing generator provides a 1.8 microsecond delay in the gated sum and produces synchronizing signals for the other parts of the particle identifier. The signals from the gated sum are fed into a function generator which raises the signal to the 1.73 power

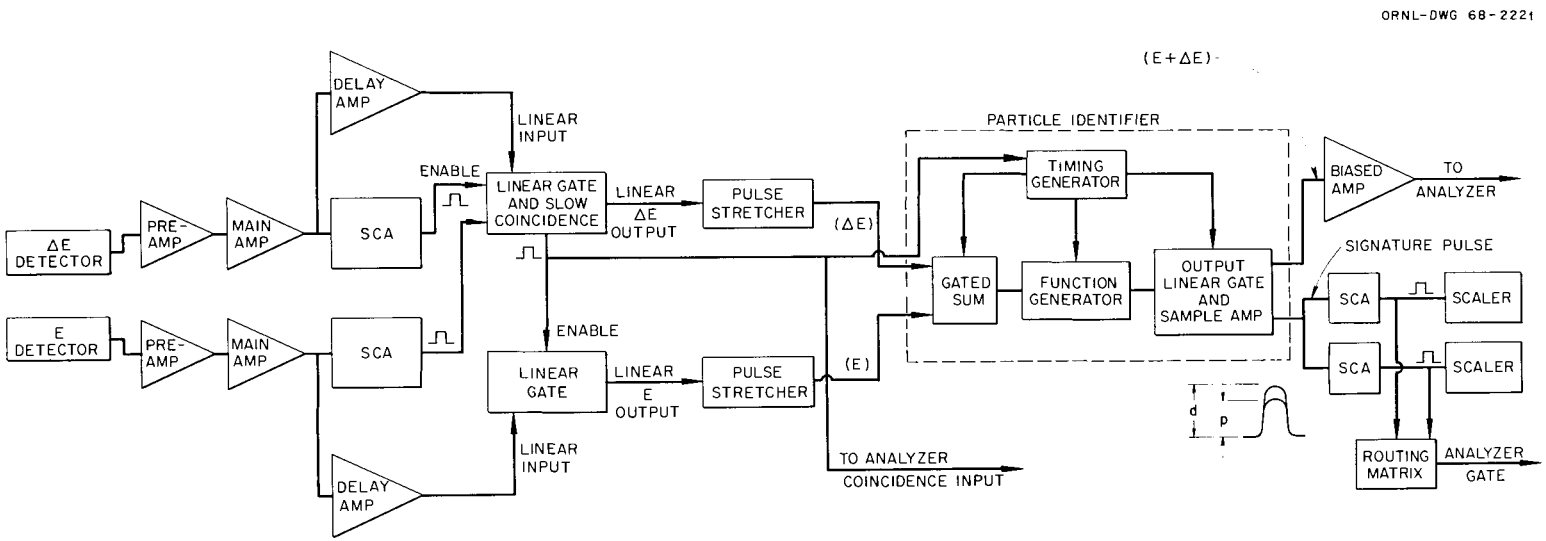

Figure 7

Particle Identification Electronics

(Figure 8). The height of the step in the output signal is given by $(E + \Delta E)^{1.73} - E^{1.73}$. This is T/A which identifies the incident particle (88).

A sample amplifier was used to pick out the step that occurs during the second 1.8 microseconds in the output signal of the function generator. After amplification to a suitable level, this pulse becomes the signature pulse (Figure 7). The total particle energy $E + \Delta E$ is obtained from the output pulse of the gated sum (88).

The signature pulses are routed through single channel analyzers whose window widths are set to allow only particles of the same type to be counted by a scaler. In this experiment, protons were counted by one scaler and deuterons were counted by the other scaler. The signals from the single channel analyzers were sent to a multichannel analyzer through a routing matrix which allowed the protons to be counted in the first 1024 channels and the deuterons in the second group of 1024 channels.

By using a pulser and dual-decade attenuator to simulate the E and ΔE detector signals, artificial beams of protons, deuterons, tritons, ^3He particles, and alphas were obtained. Figure 9 shows the separation provided for the different types of particles over the energy range considered. The E and ΔE settings on the dual-decade attenuator correspond to the E and ΔE signals obtained by using computer-calculated energy loss tables for 10-30 Mev particles and a 300-micron ΔE detector (88).

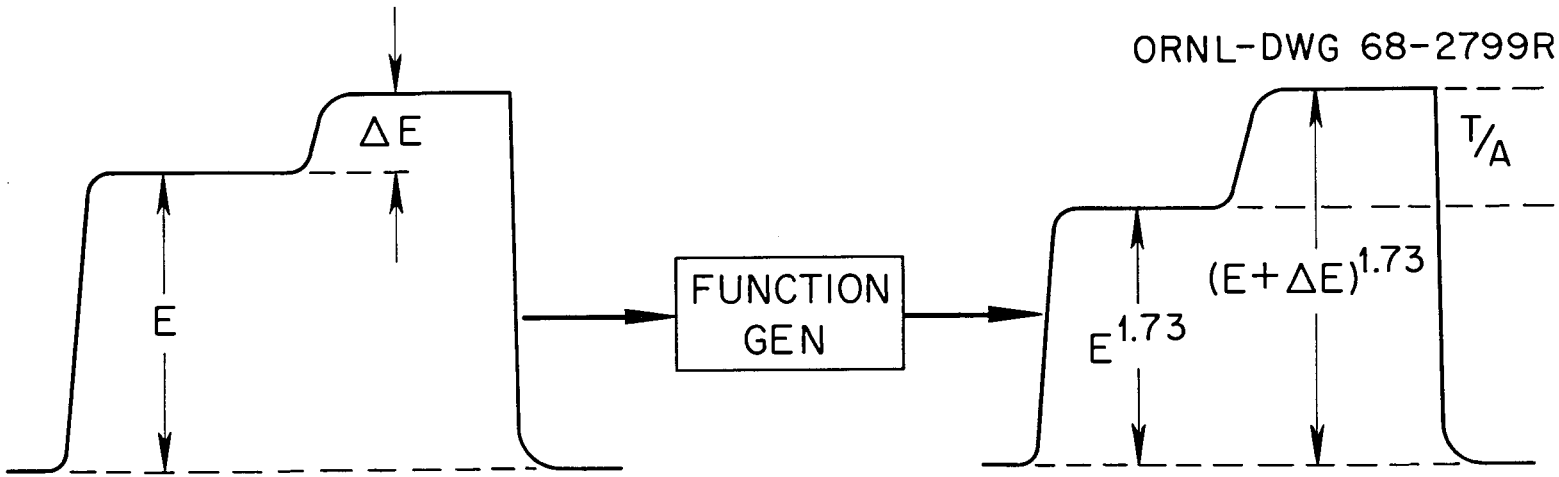

Figure 8

Diagram Illustrating Operation of the Function Generator

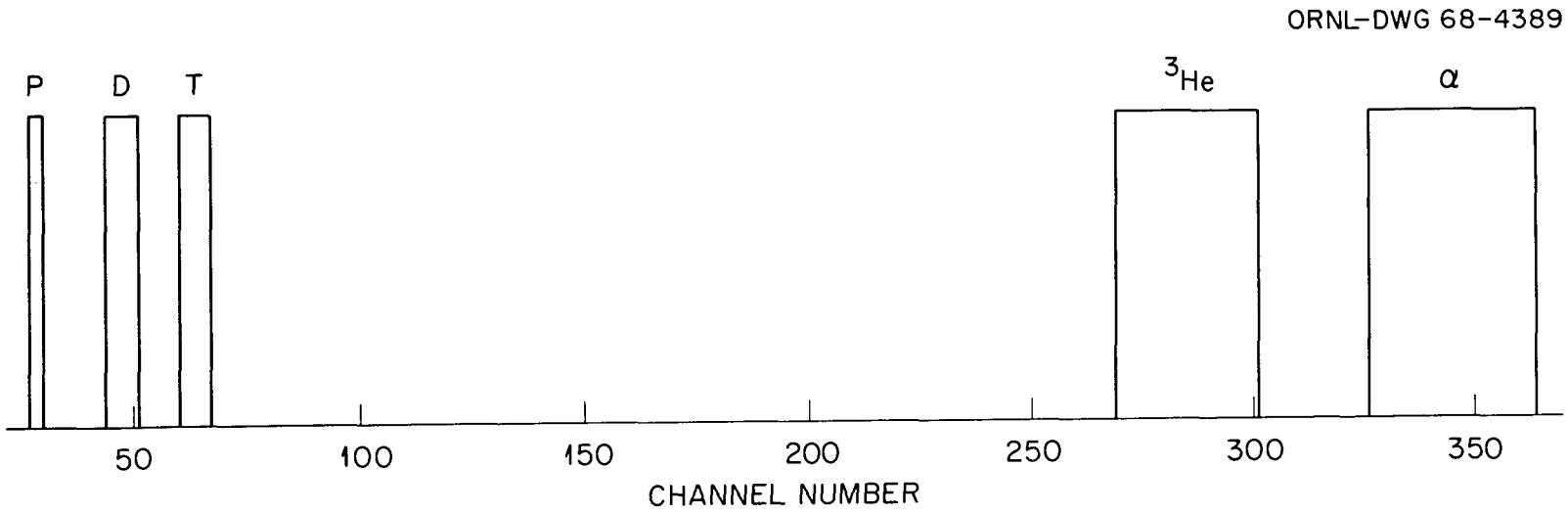

Figure 9

Particle Separation Obtained by Using Particle Identifier

V. MEASUREMENT OF BEAM CURRENT

All of the experimental measurements were made with the 5.5 Mev Van de Graaff at the Oak Ridge National Laboratory. The beam current striking the target was obtained by positioning a Faraday cup in the path of the beam. Most of the incident beam passed through the target and into the cup. The output of the Faraday cup was connected to a current integrator. After the current integrator was calibrated by using a known current, the number of ^{3}He particles passing through the target and striking the cup could be determined. A monitor detector was used to measure the elastic and inelastic groups and after each run the ratio of monitor to current integrator counts was obtained. This provided a check on the operation of the current integrator.

VI. ENERGY CALIBRATION

The pulse-height spectrum was calibrated by using an ^{241}Am alpha source and a precision pulse-height generator. As an additional check, a ^{12}C target was used and the locations of several proton groups from the $^{12}C(^{3}He,p)^{14}N$ reaction were recorded. Computer calculated kinematics were used to identify the proton groups for the $^{11}B(^{3}He,p)^{13}C$ reaction and the elastic peak for the $^{11}B(^{3}He,^{3}He)^{11}B$ reaction (89).

VII. EXPERIMENTAL DIFFERENTIAL CROSS SECTIONS

The experimental cross sections were obtained by using the expression

$$\frac{d\sigma}{dw} = \frac{n}{NN_o \Delta w} \quad , \tag{26}$$

where n is the number of integrated counts of the particle associated with the energy state, N is the number of incident ^3He ions, N_o is the number of target nuclei per cm^2, and Δw is the solid angle subtended by the detector from the target (90). The units for the experimental cross section are cm^2/steradian.

CHAPTER IV

EXPERIMENTAL RESULTS

I. EXPERIMENTAL AND THEORETICAL CROSS SECTIONS FOR PROTON DATA

The $^{11}B(^{3}He,p)^{13}C$ reaction was investigated at 10 and 12 Mev. A typical pulse-height spectrum of the proton groups corresponding to several excited states in ^{13}C is shown in Figure 10. The excited states, P_7 and P_8, corresponding to an excitation in ^{13}C of 7.50 and 7.55 Mev, are not resolved. However, for a later run the resolution was improved by using a thinner target and a thinner transmission detector and the groups were resolved. Figure 11 shows the proton angular distributions obtained for an incident ^{3}He energy of 10 Mev. The forward peaking of all the angular distributions with the exception of P_{12} is indicative of a stripping reaction.

Figures 12 and 13 show the angular distributions of P_0 and P_1 obtained for an incident ^{3}He energy of 12 Mev and Figures 14 through 20 are those angular distributions for an incident ^{3}He energy of 10 Mev. The solid curves in Figures 12 through 20 were obtained from Equation (3). The method used in calculating the transferred momentum wave number is described on pages 68 through 71 of the Appendix. The wave numbers were calculated in 5° increments from 0° to 130°. Spherical Bessel functions of order 0, 1, and 2 and reaction radii of 5-7 fermis were used to obtain the best fits to the experimental data. The square of the Bessel functions was normalized at the maximum of

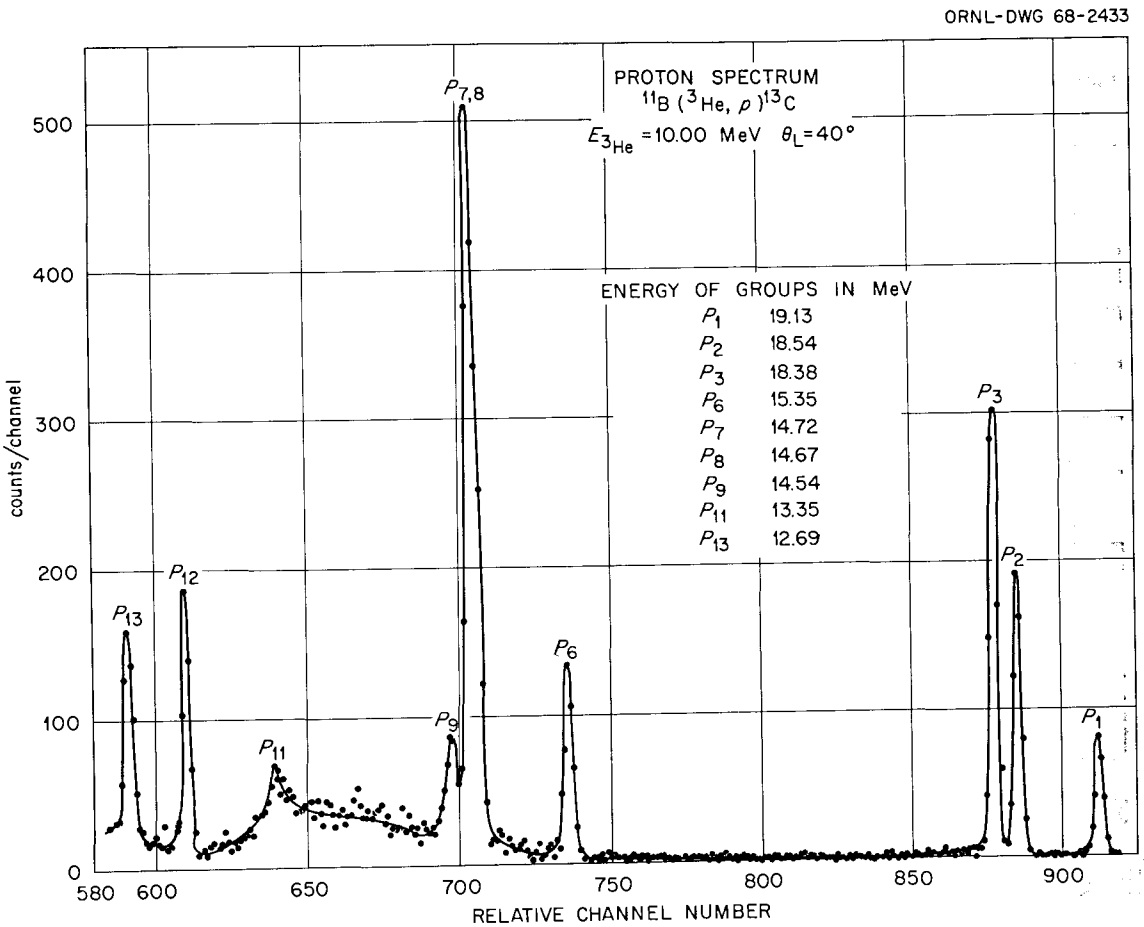

Figure 10

Pulse-Height Spectrum Showing the Proton Groups from the $^{11}B(^{3}He,p)^{13}C$ Reaction

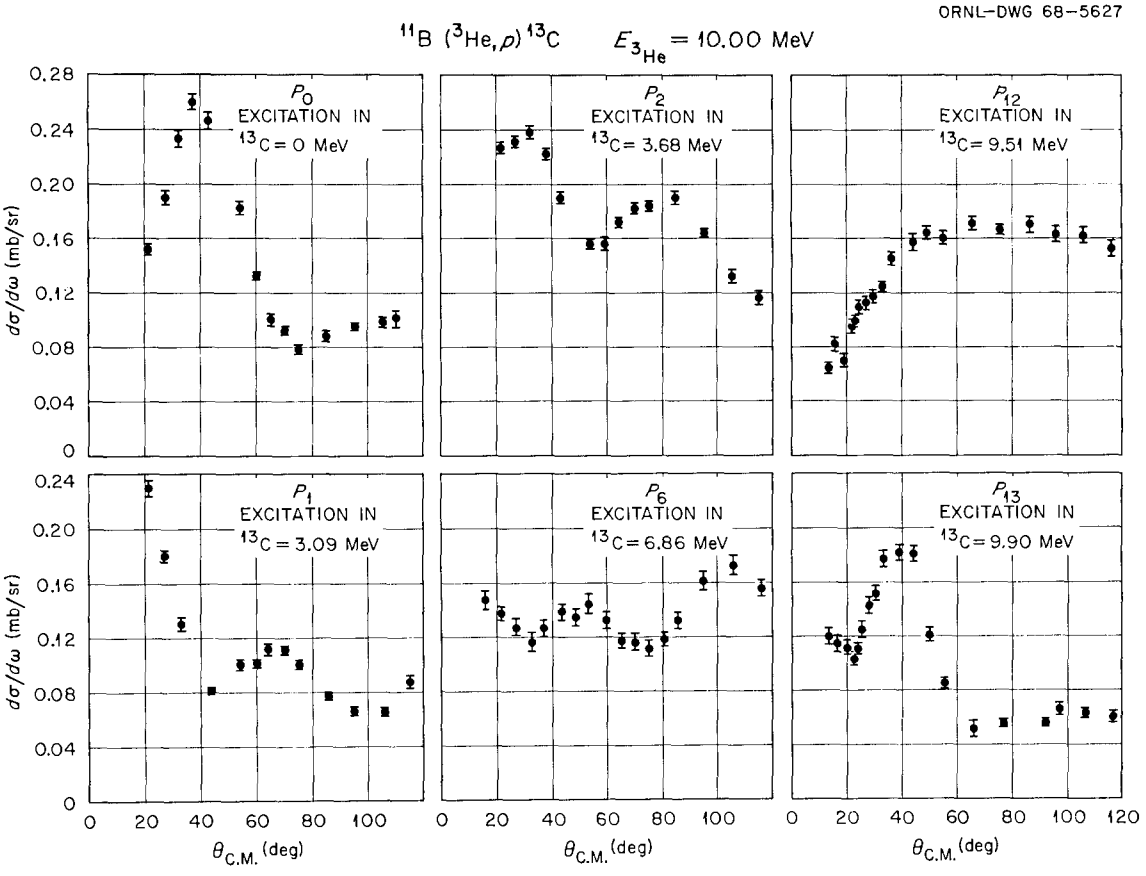

Figure 11

Angular Distributions of P_0, P_1, P_2, P_6, P_{12}, and P_{13} for $E(^{3}He)$ = 10 Mev

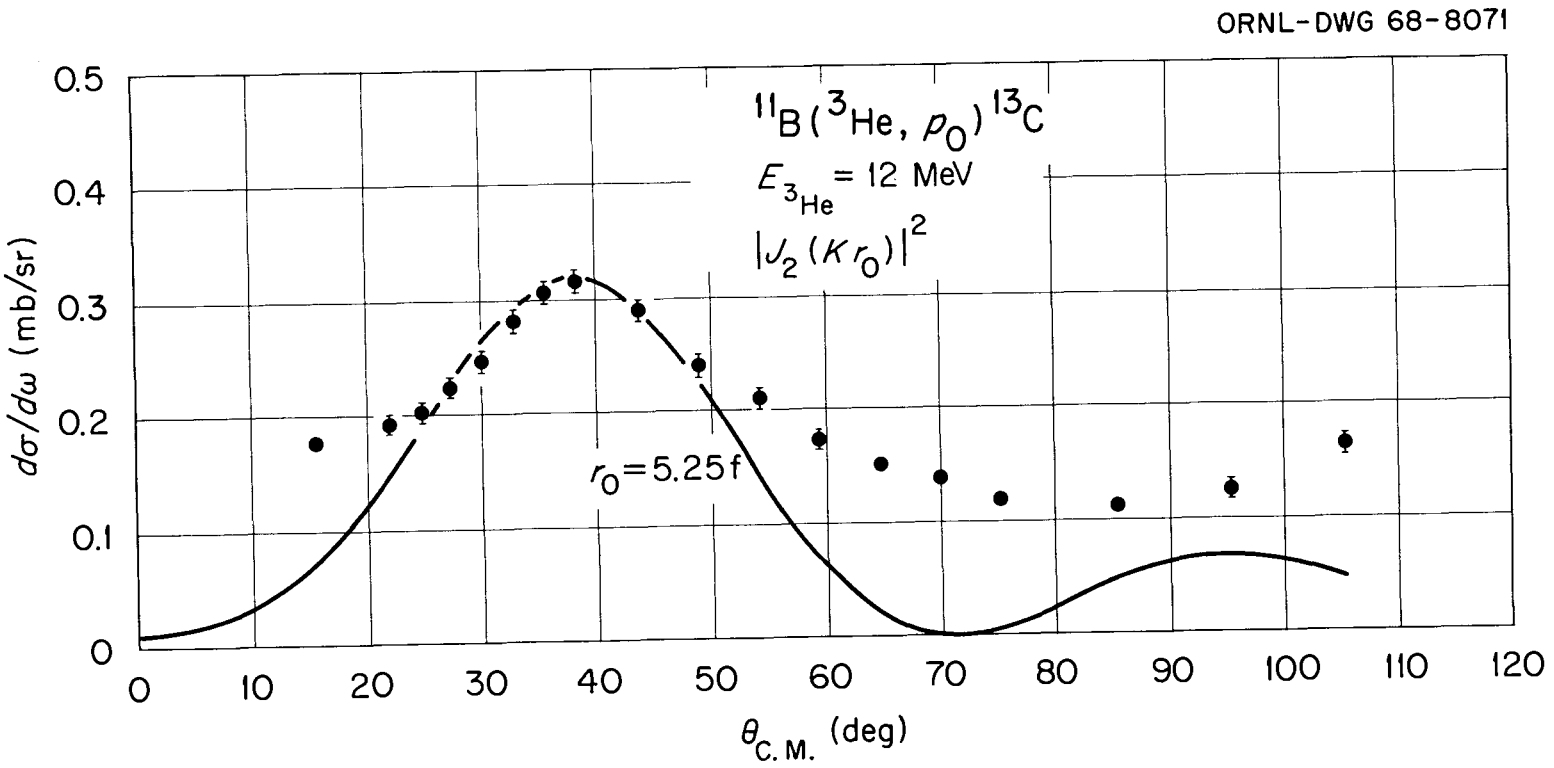

Figure 12

Angular Distribution of P_o for $E(^{3}He)$ = 12 Mev

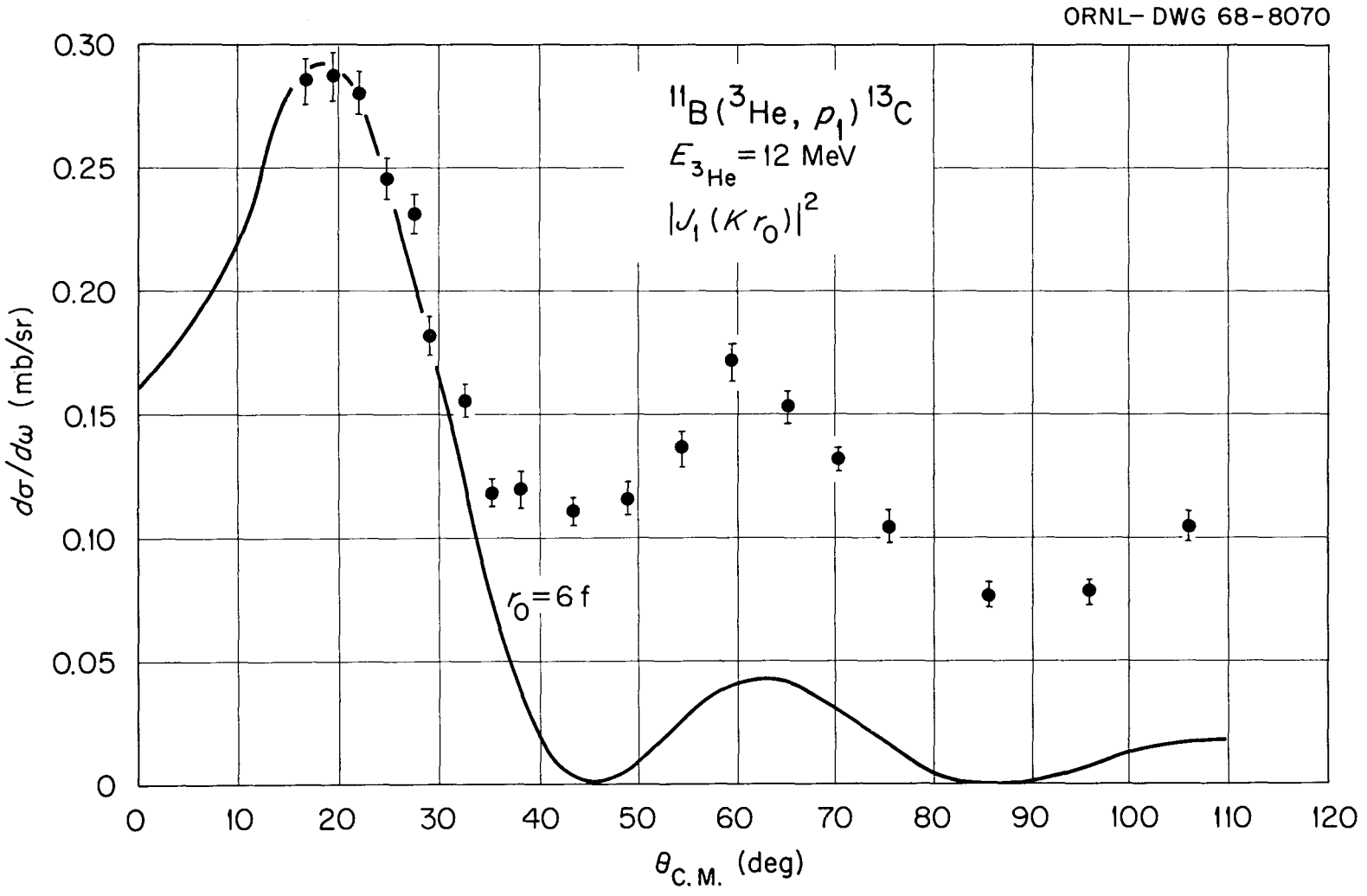

Figure 13

Angular Distribution of P_1 for $E(^3He)$ = 12 Mev

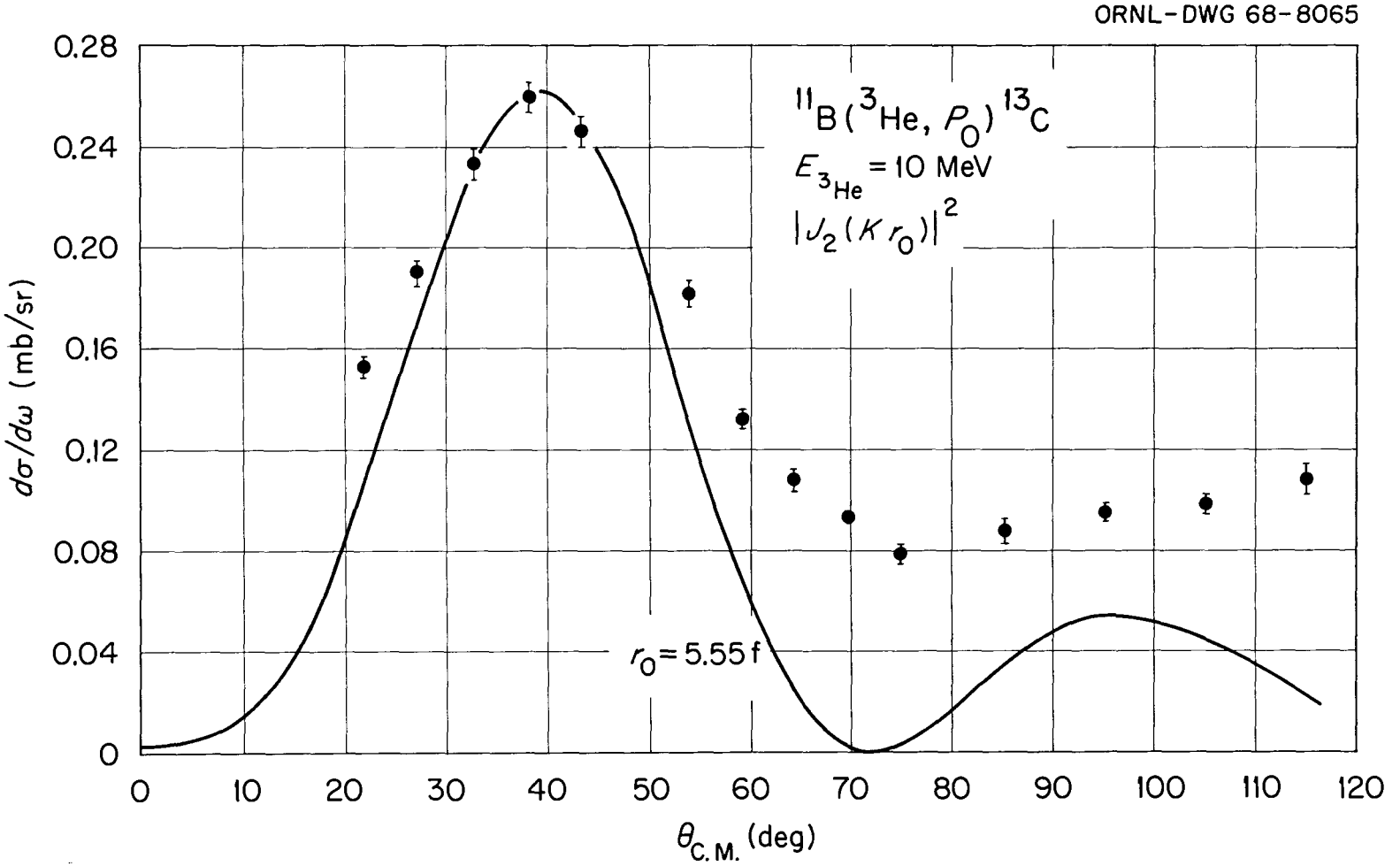

Figure 14

Angular Distribution of P_0 for $E(^3He)$ = 10 Mev

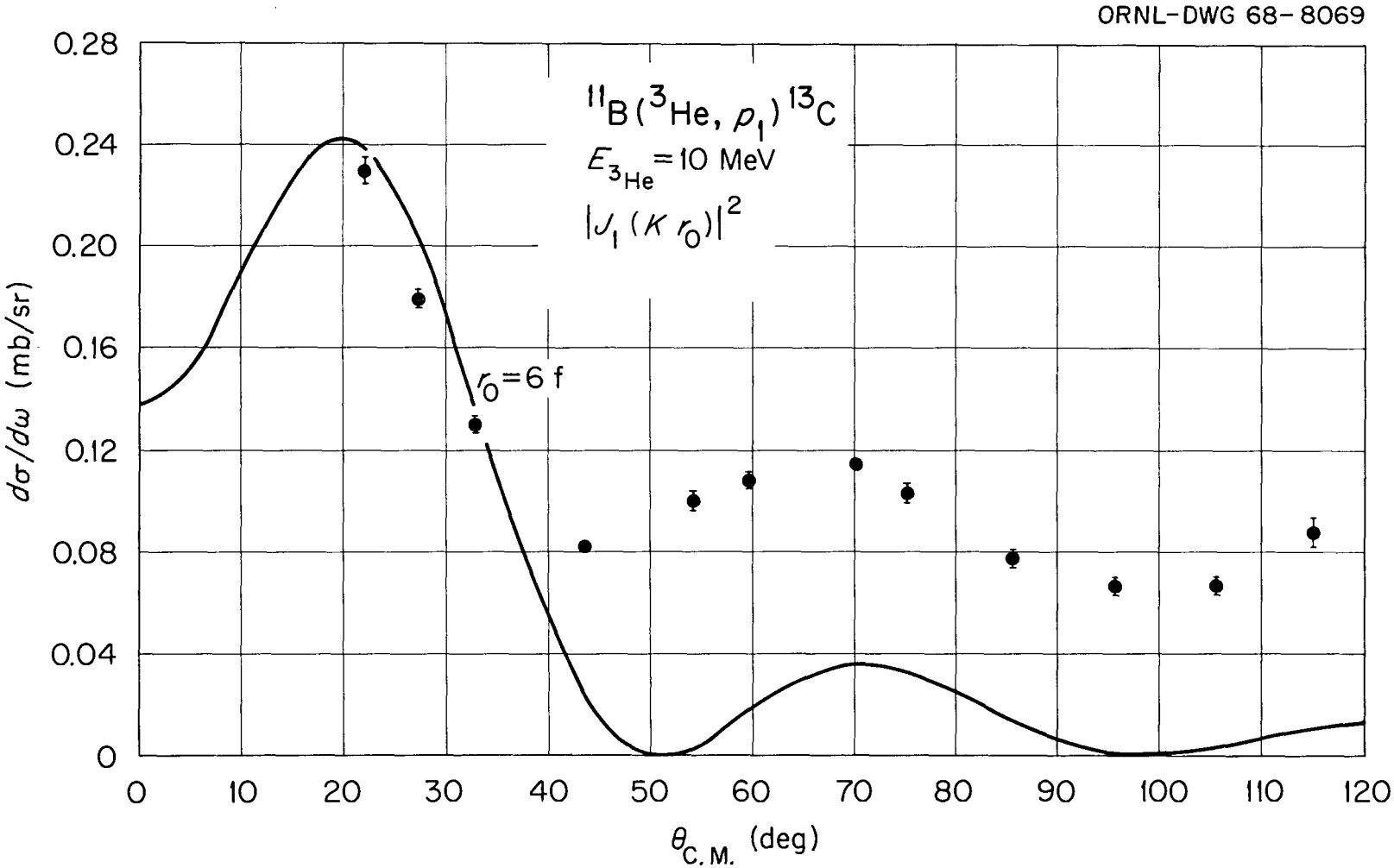

Figure 15

Angular Distribution of P_1 for $E(^3He) = 10$ Mev

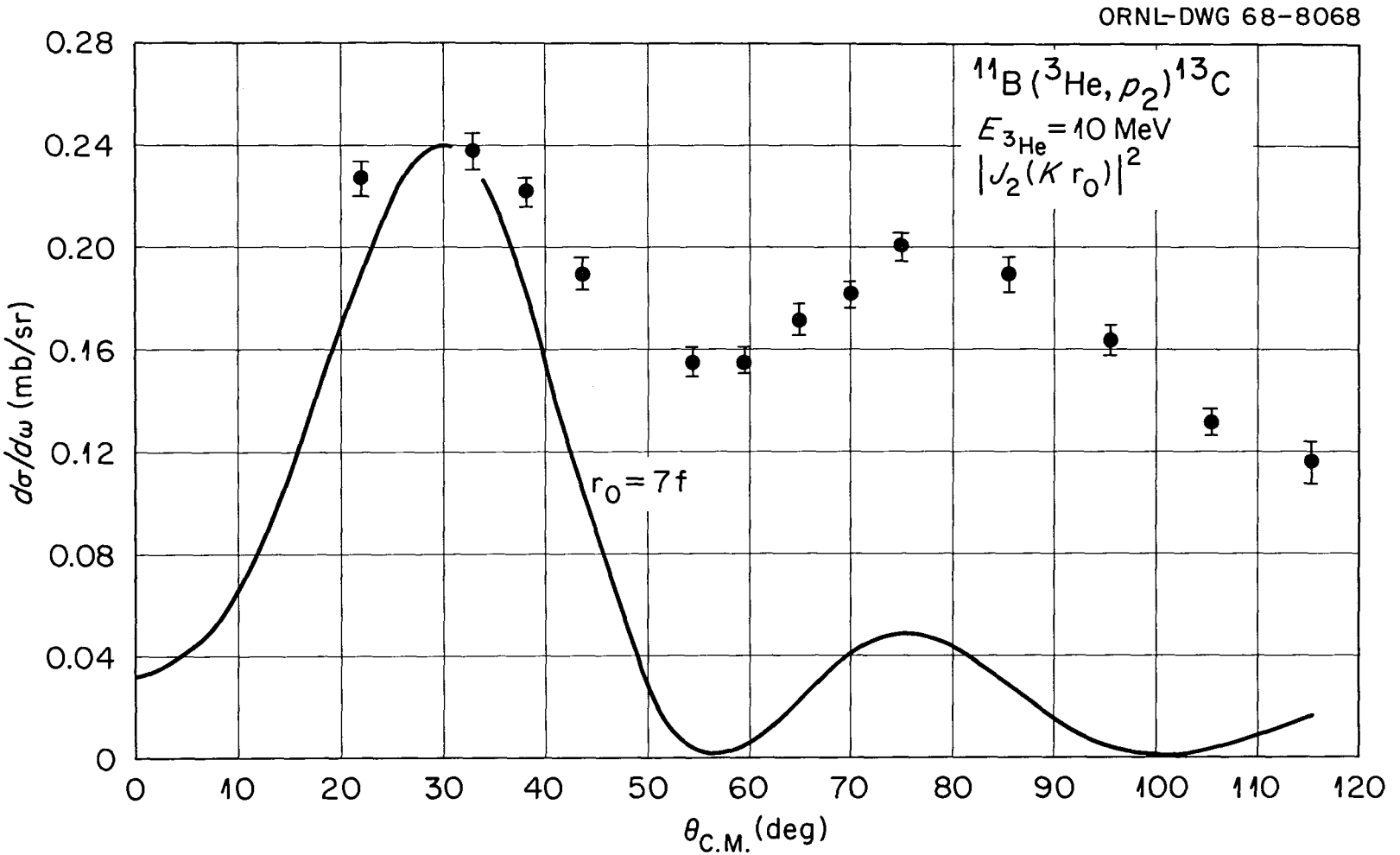

Figure 16

Angular Distribution of P_2 for $E(^{3}He)$ = 10 Mev

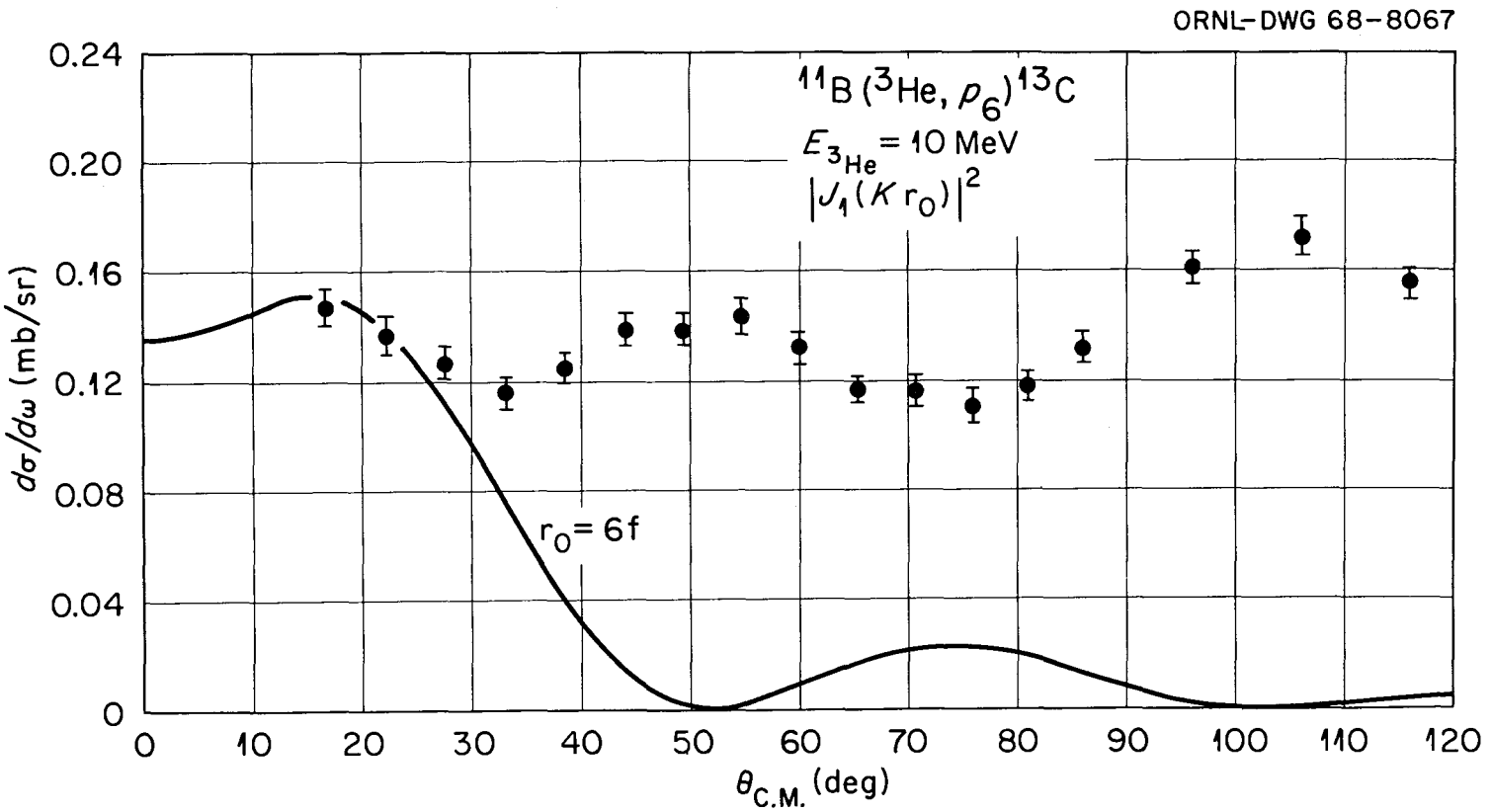

Figure 17

Angular Distribution of P_6 for $E(^3He)$ = 10 Mev

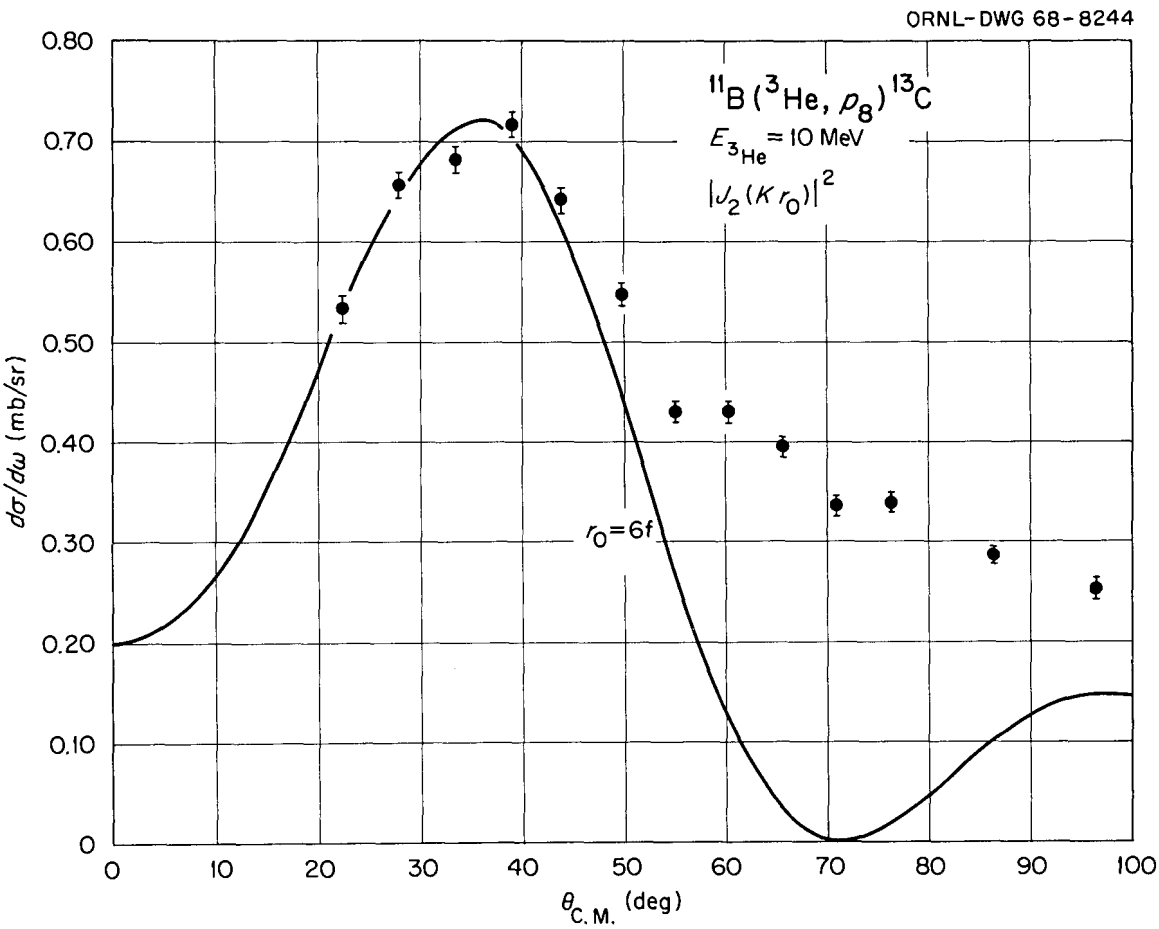

Figure 18

Angular Distribution of P_8 for E(^{3}He) = 10 Mev

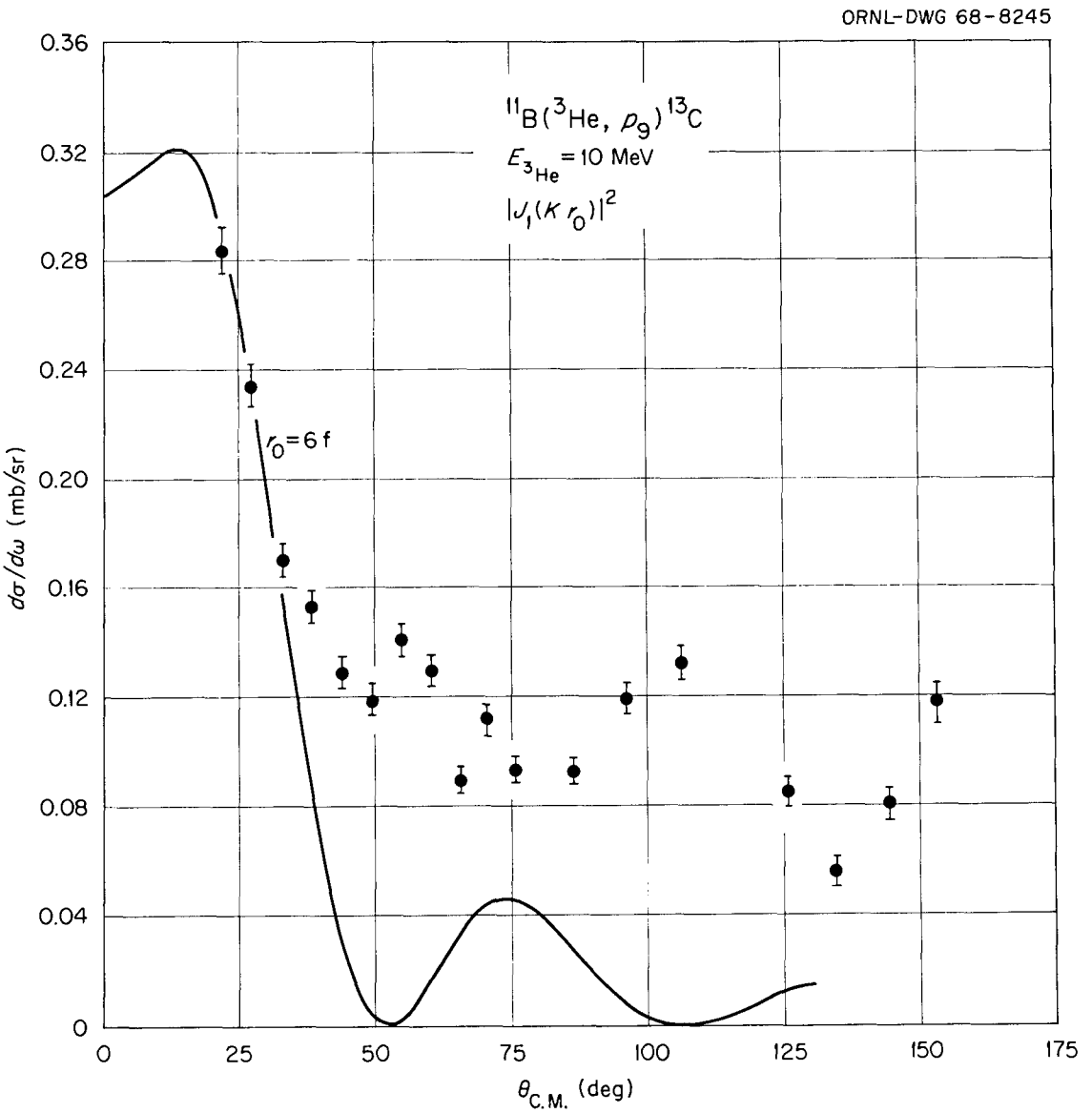

Figure 19

Angular Distribution of P_9 for E(^{3}He) = 10 Mev

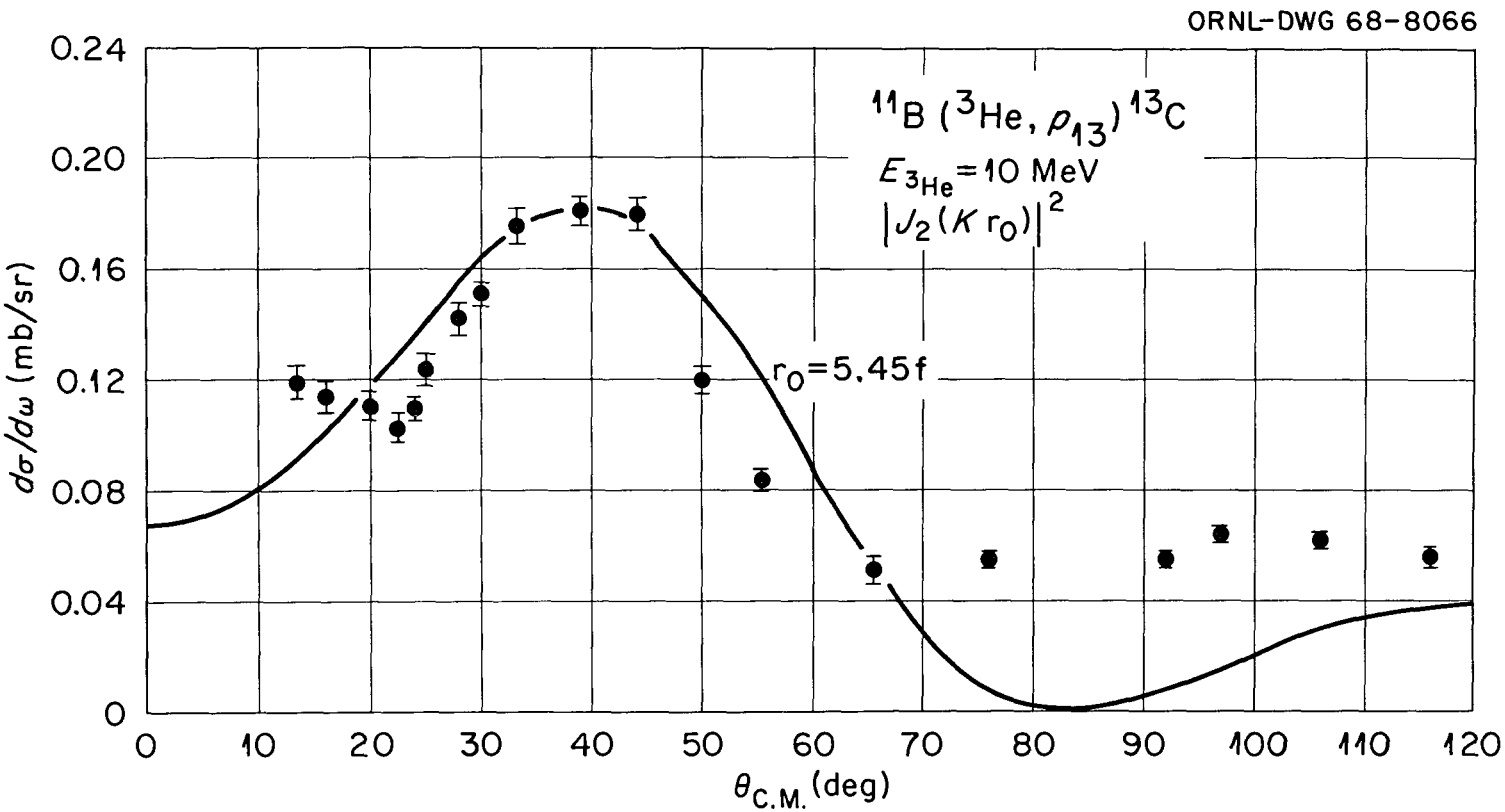

Figure 20

Angular Distribution of P_{13} for E(^{3}He) = 10 Mev

the angular distributions. The L values and reaction radii shown in Figures 12 through 20 represent those values for which the best fits were obtained. Equation (1) and the L values from the theoretical fits were used to obtain the spins and parities of the ground, first, second, sixth, eighth, ninth, and thirteenth excited states of ^{13}C.

The ground state level in ^{13}C has been assigned a spin of $\left(\frac{1}{2}\right)^-$ (91). The angular distribution for protons from the $^{11}B(^3He,p)^{13}C$ reaction for the ground state (Figures 12 and 14) indicate an L = 2 transfer which corresponds to a negative parity assignment for this level since the ground state parity for ^{11}B is negative. From Equation (1), the range of the angular momentum values is $\left(\frac{9}{2}, \frac{7}{2}, \frac{5}{2}, \frac{3}{2}, \frac{1}{2}\right)^-$. McGruer, Warburton, and Bender obtained a spin and parity of $\left(\frac{3}{2}, \frac{1}{2}\right)^-$ for the ground state in ^{13}C from the $^{12}C(d,p)^{13}C$ reaction for an incident deuteron energy of 14.8 Mev (92). Figures 13 and 15 indicate an L = 1 transfer for the first excited state of ^{13}C. This results in a positive parity assignment and a range of angular momentum values of $\left(\frac{7}{2}, \frac{5}{2}, \frac{3}{2}, \frac{1}{2}\right)^+$ which is in accord with the values found in References 91 and 92.

Ajzenberg-Selove and Lauritsen (91) list a spin and parity of $\left(\frac{3}{2}\right)^-$ and $\frac{3}{2}^+$ for the second and ninth excited states of ^{13}C, respectively. Figures 16 and 19 indicate an L value of 2 for P_2 and 1 for P_9. This results in a spin and parity assignment of $\left(\frac{9}{2}, \frac{7}{2}, \frac{5}{2}, \frac{3}{2}, \frac{1}{2}\right)^-$ for P_2 and $\left(\frac{7}{2}, \frac{5}{2}, \frac{3}{2}, \frac{1}{2}\right)^+$ for P_9. Rotblat (93) and McGruer, Warburton and Bender (92) obtained a spin and parity of $\left(\frac{1}{2}, \frac{3}{2}\right)^-$ for P_2 from the $^{12}C(d,p)^{13}C$ reaction. The best fit for the proton angular distribution from the

sixth excited state in ^{13}C was obtained for an L value of 1. This corresponds to a spin and parity assignment of $\left(\frac{7}{2}, \frac{5}{2}, \frac{3}{2}, \frac{1}{2}\right)^{+}$ which encompasses the value $\frac{5^{+}}{2}$ listed in Reference 91. Figures 18 and 20, pages 47 and 49, show the angular distributions of protons from the eighth and thirteenth excited states in ^{13}C, respectively. The L values correspond to a spin and parity assignment of $\left(\frac{9}{2}, \frac{7}{2}, \frac{5}{2}, \frac{3}{2}, \frac{1}{2}\right)^{-}$ for both states. Spin and parity values for the eighth and thirteenth excited states have not been reported.

II. ELASTIC SCATTERING DATA

Figure 21 shows the electronic schematic used to simultaneously monitor the elastically scattered ^{3}He particles from the $^{11}B(^{3}He,^{3}He)^{11}B$ reaction and the protons from the $^{11}B(^{3}He,p)^{13}C$ reaction for an incident ^{3}He energy of 12 Mev. The 10 Mev proton data were obtained by using the electronic schematic shown in Figure 7 on page 32. The 8 and 10 Mev elastically scattered ^{3}He data were obtained in separate runs by monitoring only the ^{3}He pulses from the ΔE detector.

Figures 22 through 24 show the angular distributions obtained for the elastically scattered ^{3}He particles at 8, 10, and 12 Mev. The solid curves represent optical model fits obtained by J. Y. Park at North Carolina State University. A brief description of the optical model analysis of elastic scattering is covered on pages 12 through 15 of Chapter II.

Figure 22 shows the angular distribution of the 8 Mev elastically scattered ^{3}He particles. The solid curve represents an optical model

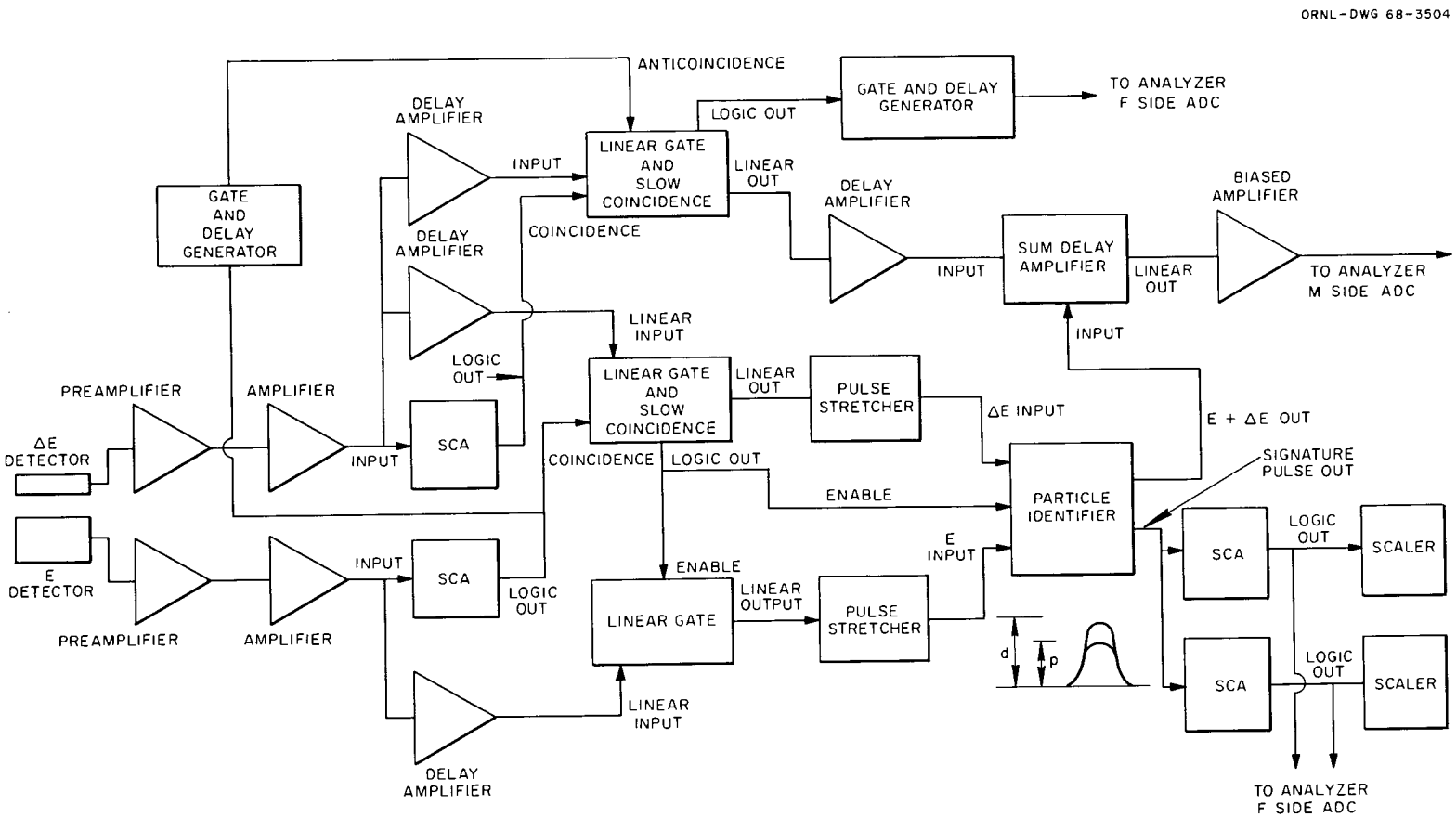

Figure 21

Electronic Schematic Used in Taking 12 Mev Data

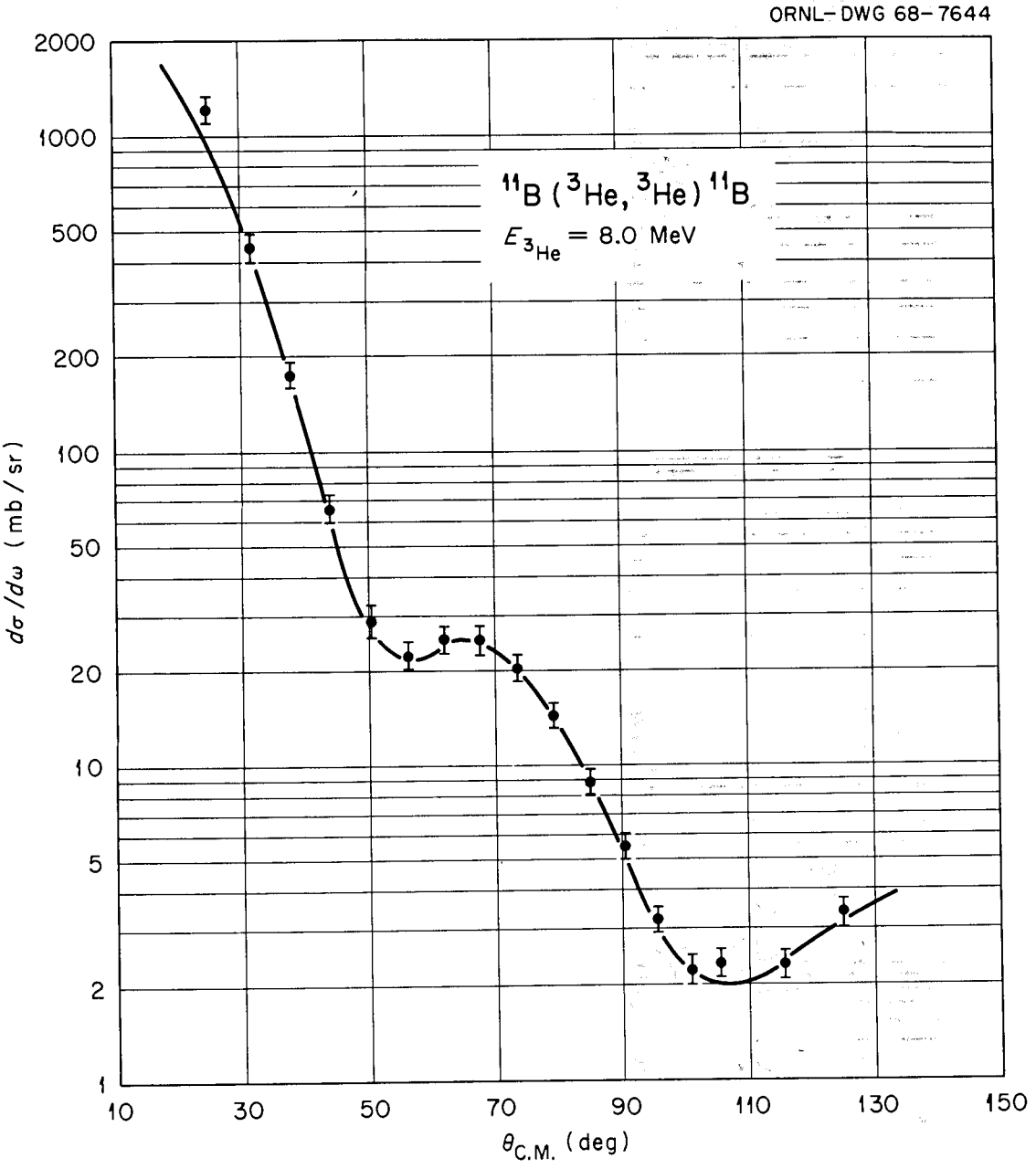

Figure 22

Angular Distribution of Elastically Scattered ^{3}He Particles for $E(^{3}He) = 8$ Mev

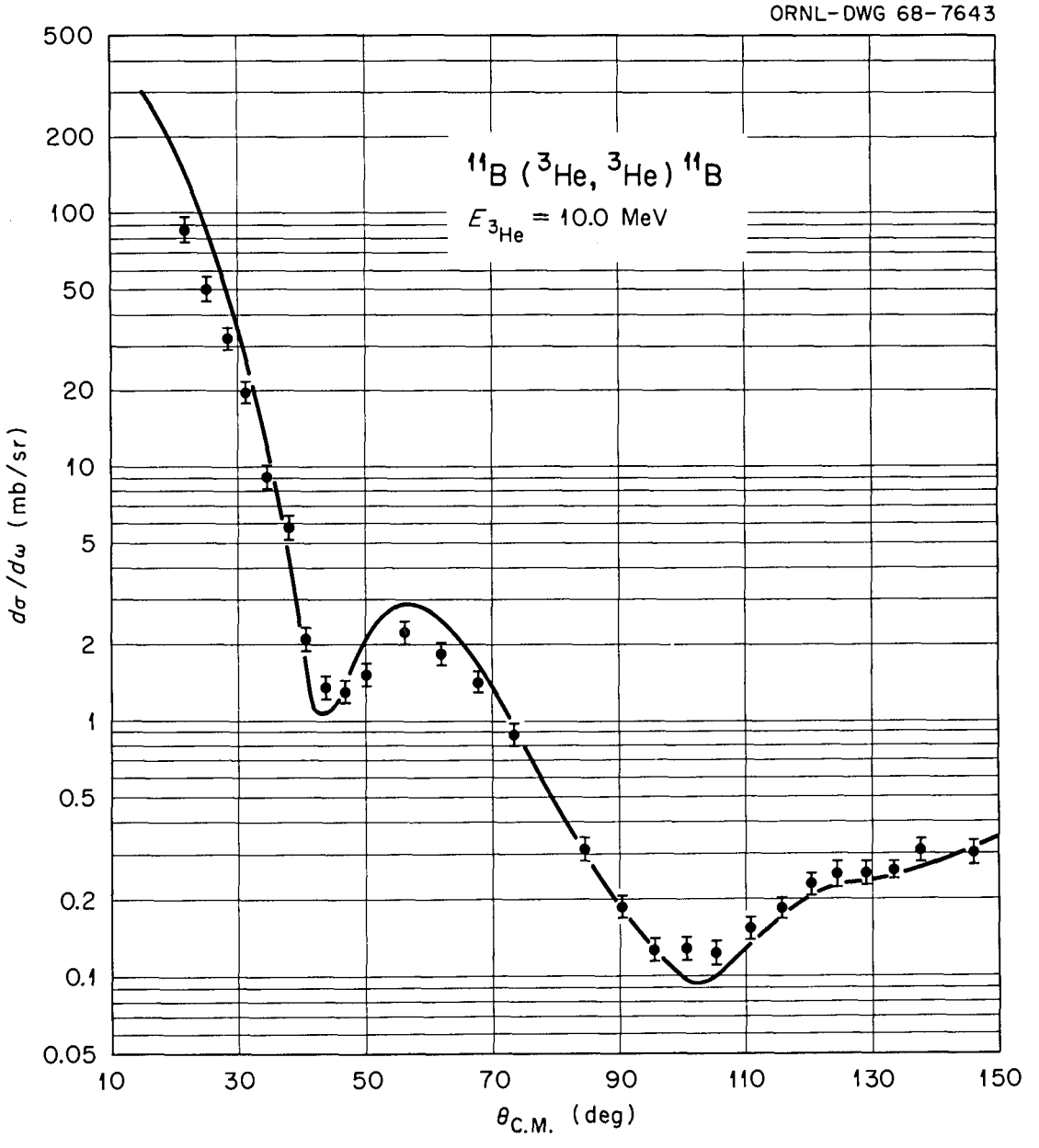

Figure 23

Angular Distribution of Elastically Scattered ^{3}He Particles for $E(^{3}He)$ = 10 Mev

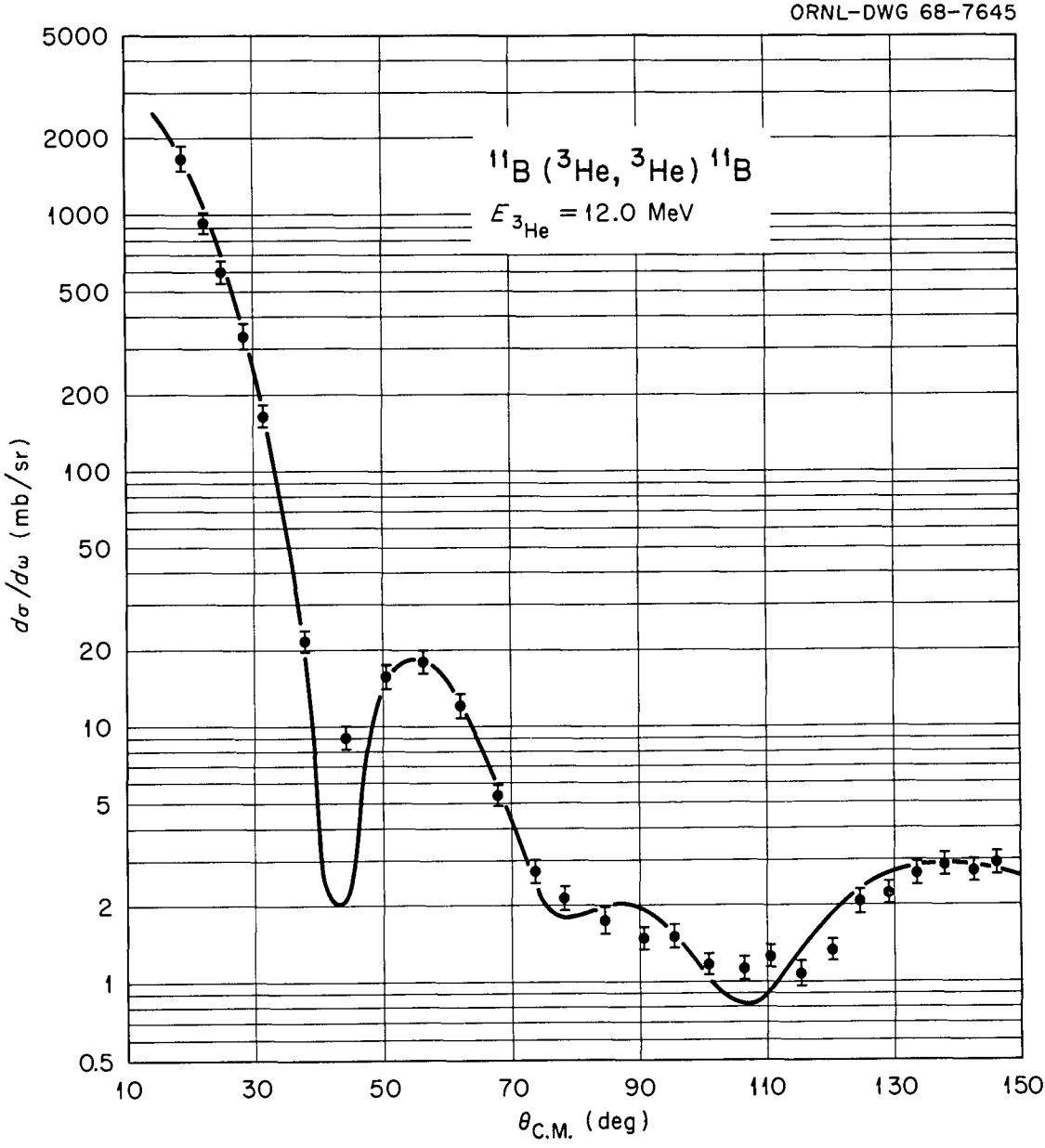

Figure 24

Angular Distribution of Elastically Scattered ^{3}He Particles for $E(^{3}He)$ = 12 Mev

fit using volume absorption with spin-orbit coupling. The best fit was obtained with the parameters

$$V = 139.0 \text{ Mev},$$

$$W = 15.0 \text{ Mev},$$

$$r_o = 1.2 \text{ fermis},$$

$$r_c = 1.4 \text{ fermis},$$

$$V_s = 7.5 \text{ Mev},$$

$$W_s = 0.0 \text{ Mev},$$

$$a = 0.65 \text{ fermis},$$

where V and W are the real and imaginary parts of the central nuclear potential, r_o is the nuclear radius, r_c is the Coulomb radius parameter, "a" is the diffuseness of the nuclear surface, and V_s and W_s are the real and imaginary parts of the spin-orbit potential.

Surface absorption without spin-orbit coupling was used to fit the 10 Mev data shown in Figure 23. The parameters used were

$$V = 136.5 \text{ Mev},$$

$$W = 14.0 \text{ Mev},$$

$$r_o = 1.2 \text{ fermis},$$

$$r_c = 1.4 \text{ fermis},$$

$$r_{o_g} = 1.2 \text{ fermis},$$

$$a = 0.74 \text{ fermis},$$

$$b = 1.40 \text{ fermis},$$

where r_{o_g} is the nuclear Gaussian radius, b is the width of the Gaussian, and the other terms are the same as for Figure 22.

Surface absorption with spin-orbit coupling was used to fit the 12 Mev data shown in Figure 24, page 55. The parameters used were

$V = 121.0$ Mev,

$W = 10.0$ Mev,

$r_o = 1.2$ fermis,

$r_c = 1.4$ fermis,

$r_{o_g} = 1.2$ fermis,

$V_s = 4.0$ Mev,

$W_s = 0.0$ Mev,

$a = 0.75$ fermis,

$b = 1.75$ fermis,

where the terms are as defined on page 56.

IV. ERRORS IN CROSS SECTION MEASUREMENTS

The error bars in Figures 12 through 20 and 22 through 24, pages 41 through 49 and 53 through 55, represent the statistical variation. Other major sources of error are the target thickness which was discussed on pages 21 through 25 of Chapter III and the measurement of the acceptance angle from which the solid angle was calculated. A traveling light microscope was used in measuring the parameters used in calculating the solid angle. By this method an acceptance angle of 0.490° was obtained. Elastically scattered ^3He particles at a lab angle of 70° and an energy of 12 Mev were used to check the acceptance angle measurement. From the equation

$$(\Delta E)^2 = (\Delta E_e)^2 + (\Delta E_T)^2 + (\Delta E_K)^2 \quad , \qquad (27)$$

where ΔE is the measured resolution, ΔE_e is the electronic resolution, and ΔE_T is the spread due to target thickness, the kinematic spread, ΔE_K, can be calculated. Figure 25 shows the elastic peak and from the peak the measured resolution was determined to be 45.6 kev. The electronic resolution of 25.2 kev was obtained by using a precision pulse-height generator. The spread due to target thickness was obtained by multiplying the stopping power for 12 Mev ^{3}He particles by the target thickness in micrograms/cm^2. The resulting spread was 37.2 kev. Substituting the values in Equation (27) gave a spread due to kinematics of 35.4 kev. From the kinematics, the ^{3}He particles have a spread of ~79 kev/degree at 70°. By dividing the energy spread per degree of the ^{3}He elastics at 70° into the kinematic energy spread gave an acceptance angle of 0.448°. The difference between the two angular measurements is 8.6 percent. However, the value obtained by using the traveling light microscope was used and is believed to be accurate to ±5 percent. Thus, in addition to the statistical error, the absolute cross sections could vary ±15 percent due to errors in foil thickness measurements and ±5 percent due to the acceptance angle measurement.

V. CONCLUSIONS

The fitting of the elastic data for the ^{11}B(^{3}He,^{3}He)^{11}B reaction indicates that the optical model can be used to describe the experimental results and provide information about the distorting potentials that can be used for distorted wave calculations. The forward peaking

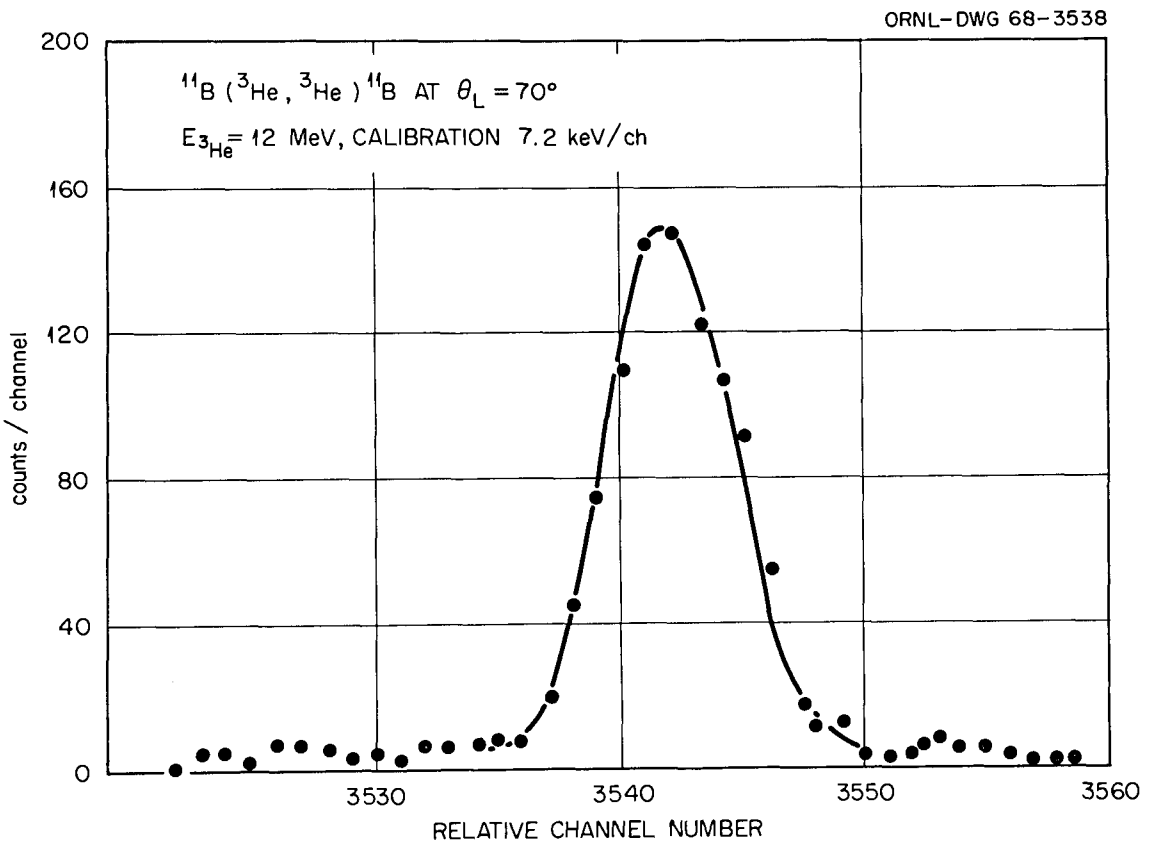

Figure 25

Pulse-Height Spectrum for Elastically Scattered ^{3}He Particles

for most of the angular distribution curves for the proton groups from the $^{11}B(^{3}He,p)^{13}C$ reaction indicate that the predominant reaction mechanism is stripping for incident ^{3}He energies of 10 and 12 Mev. Using the plane wave stripping formalism of Newns (13), spin and parity assignments were made for several excitation levels in ^{13}C.

LIST OF REFERENCES

LIST OF REFERENCES

1. Leighton, R. B., Principles of Modern Physics, (McGraw-Hill Book Company, Inc., New York, 1959), pp. 562-564.

2. Evans, R. D., The Atomic Nucleus, (McGraw-Hill Book Company, Inc., New York, 1955), p. 90.

3. Butler, S. T., Nuclear Stripping Reactions, (John Wiley and Sons, Inc., New York, 1957), p. 1.

4. Blatt, J. M., and Weisskopf, V. F., Theoretical Nuclear Physics, (John Wiley and Sons, Inc., New York, 1952), p. 340.

5. Moszkowski, S. A., University of California Report No. UCRL-5701, Los Angeles, (1958), pp. 7-8.

6. Burcham, W. E., Nuclear Physics, An Introduction, (McGraw-Hill Book Company, Inc., New York, 1963), p. 556.

7. Reference 5, pp. 10-11.

8. Park, J. Y., "The Theory of Direct Nuclear Knock-Out Reactions," (Dissertation, The University of North Carolina, Chapel Hill, 1962), p. 5.

9. Reference 3, p. 7.

10. Huby, R., Proc. Roy. Soc. (London), A215, 385 (1952).

11. Tobocman, W., Technical Report No. 29, Case Institute of Technology, Cleveland, (1956).

12. Butler, S. T., Phys. Rev., 106, 272 (1957).

13. Newns, H. C., Proc. Phys. Soc., A76, 489 (1960).

14. el Nadi, M., Phys. Rev., 119, 242 (1960).

15. Bromley, D. A., and Almqvist, E., Chalk River Report CRP 881, Atomic Energy of Canada Limited (1959), p. 559.

16. Allen, K. W., Almqvist, E., and Bigham, C. B., Phys. Rev., 99, 631 (1955).

17. Almqvist, E., et al., Phys. Rev., 91, 1022 (1953).

18. Almqvist, E., et al., Phys. Rev., 114, 1040 (1959).

19. Almqvist, E., et al., Phys. Rev., 105, 957 (1957).

20. Johnston, R. L., et al., Phys. Rev., 109, 884 (1958).

21. Moak, C. D., et al., Phys. Rev., 110, 1369 (1958).

22. Moak, C. D., and Wisseman, W. R., Phys. Rev., 101, 1326 (1956).

23. Sweetman, D. R., Bull. Am. Phys. Soc., 3, 186 (1958).

24. Wegner, H. E., and Hall, W. S., Bull. Am. Phys. Soc., 3, 338 (1958).

25. Coker, W. R., et al., Nucl. Phys., 91, 97 (1967).

26. Reference 15, pp. 577-587.

27. Galonsky, A., et al., Bull. Am. Phys. Soc., 2, 51 (1957).

28. Holmgren, H. D., Wolicki, E. A., and Johnston, R. L., Bull. Am. Phys. Soc., 2, 181 (1957).

29. Marsh, B. B., and Bilaniuk, O. M., Phys. Rev., 130, 2373 (1963).

30. Gallmann, A., et al., Phys. Rev., 129, 1765 (1962).

31. Young, T. E., et al., Phys. Rev., 116, 962 (1959).

32. Hunting, C. E., and Wall, N. S., Phys. Rev., 115, 956 (1959).

33. von Herrmann, P., and Pieper, G. F., Phys. Rev., 105, 1556 (1957).

34. Ivascu, M., Dumitrescu, R., and Semenescu, G., Revue Roumaine de Physique, 12, 279 (1967).

35. Yamazki, T., Kondo, M., and Yamabe, S., Jap. Phys. Soc., 18, 620 (1963).

36. Pieper, G. F., and Stanford, G. S., Phys. Rev., 101, 672 (1956).

37. Reference 34, p. 282.

38. Satchler, G. R., Nucl. Phys., 55, 1 (1964).

39. Tobocman, W., Theory of Direct Nuclear Reactions, (Oxford University Press, New York, 1961), pp. 25-40.

40. Igo, G., and Thaler, R. M., Phys. Rev., 107, 1343 (1957).

41. Halbert, M. L., Hunting, C. E., and Zucker, A., Phys. Rev., 117, 1545 (1960).

42. Glassgold, A. E., et al., Phys. Rev., 106, 1207 (1957).

43. Melkanoff, M. A., et al., Phys. Rev., 106, 793 (1957).

44. Glassgold, A. E., and Kellogg, P. J., Phys. Rev., 107, 1372 (1957).

45. Glassgold, A. E., Optical Model for Nuclear Scattering, Vol. VII of Progress in Nuclear Physics, O. R. Frisch (ed.), 9 Vols., (Pergamon Press, New York, 1959), p. 156.

46. Aguilar, J., et al., Proc. Roy. Soc., A257, 13 (1960).

47. Parry, G., Scott, H. D., and Swierszczewski, S., Proc. Phys. Soc., 77, 230 (1961).

48. Greenlees, G. W., and Rowe, P. C., Nucl. Phys., 15, 687 (1960).

49. Weller, H. R., Robertson, N. R., and Tilley, D. R., Bull. Am. Phys. Soc., 12, 518 (1967).

50. Kellog, E. M., and Zurmukle, R. W., Phys. Rev., 152, 890 (1966).

51. Park, J. Y., "Optical Model Analysis of Elastic Scattering of ^{3}He Particles by ^{12}C in the Range of 3.7 to 15 Mev," (unpublished report, North Carolina State University, Raleigh, 1967), p. 12.

52. Hodgson, P. E., Nucl. Phys., 21, 28 (1960).

53. Reference 15, p. 617.

54. Reference 3, p. 6.

55. Reference 10, p. 186.

56. Reference 3, pp. 5-6.

57. Reference 45, p. 124.

58. Reference 45, p. 125.

59. LeLevier, R., and Saxon, D. S., Phys. Rev., 87, 40 (1952).

60. Feshbach, H., Porter, C. E., and Weisskopf, V. F., Phys. Rev., 96, 448 (1954).

61. Chase, D. M., and Rohrlich, F., Phys. Rev., 94, 81 (1954).

62. Woods, R. W., and Saxon, D. S., Phys. Rev., 95, 577 (1954).

63. Reference 51, p. 2.

64. Buck, B., Maddison, R. N., and Hodgson, P. E., Phil. Mag., 5, 1181 (1960).

65. Muggleton, A. H. F., and Howe, F. A., Nucl. Instr. Methods, 13, 211 (1961).

66. Adair, H. L., and Kobisk, E. H., "Boron Film Preparation Using an Electron Evaporator," The Ninth National Vacuum Symposium, American Vacuum Society, Los Angeles, California, (1962), p. 125.

67. Hoke, G. R., and Newman, E., "Self-Supported Cyclotron Targets of Boron and Magnesium," ORNL-3021, Oak Ridge National Laboratory, (1961).

68. O'Bryan, H. M., Rev. Sci. Instr., 5, 125 (1934).

69. Flinta, J., Vacuum, 2, 257 (1960).

70. Barnes, D., Mackenzie, R. B., and Aves, R., "Boron Films," AERE Rpt. R/M-125, Harwell, England, (1957).

71. Dodson, R. W., et al., "Preparation of Foils," in Miscellaneous Physical and Chemical Techniques of the Los Alamos Project, A. C. Graves and D. K. Froman (eds.), (McGraw-Hill Book Company, Inc., New York, 1952), pp. 19-22.

72. Korsunsky, M., and Vekshinsky, S., J. of Phys., 9, 399 (1945).

73. Adair, H. L., and Kobisk, E. H., "Formation of Thin Films and Other Forms of Isotopic Metal by Electron Bombardment Evaporation," Proceedings of the Electron Beam Symposium, Sixth Annual Meeting, Boston, Massachusetts, (1964), p. 206.

74. Livingston, M. S., and Bethe, H. A., Rev. Mod. Phys., 9, 263 (1937).

75. Booth, W., and Grant, I. S., Nucl. Phys., 63, 481 (1965).

76. Whaling, Ward, Handbuch der Physik, Vol. 34, S. Flugge (ed.), (Springer-Verlag, Berlin, 1958), pp. 193-217.

77. Wolke, R. L., et al., Phys. Rev., 129, 2591 (1963).

78. Northcliffe, L. C., Phys. Rev., 120, 1744 (1960).

79. Williamson, Claude Finley, Boujot, Jean-Paul, and Picard, Jean, "Tables of Range and Stopping Power of Chemical Elements for Charged Particles of Energy 0.05 to 500 Mev," French Rpt. CEA-R 3042, (1966).

80. Whaling, Ward, and Li, C. W., Phys. Rev., 81, 661 (1951).

81. Van Heerden, P. J., "The Crystal Counter," (Dissertation, University of Utrecht, Netherlands, 1945), p. 16.

82. Miller, G. L., The Physics of Semiconductor Radiation Detectors, BNL-699, Brookhaven National Laboratory, (1961).

83. Reference 6, p. 213.

84. Oak Ridge Technical Enterprises Corporation, Catalog 1000, Oak Ridge, Tennessee, 1966, p. 60.

85. Weiss, Bill, Oak Ridge Technical Enterprises Corporation, private communication, March, 1968.

86. Goulding, F. S., et al., IEEE Trans. Nucl. Sci., 11, 388 (1964).

87. Chaminade, R., Farnce, J. C., and Pain, J., Nucl. Instr. Methods, 49, 217 (1967).

88. Oak Ridge Technical Enterprises Corporation, Particle Identifier (Instruction Manual 423), Oak Ridge, Tennessee, 1966.

89. Ball, J. B., Kinematics 11: A Nonrelativistic Kinematics Fortram Program to Aid Analysis of Nuclear Reaction Angular Distribution Data, ORNL-3251, Oak Ridge National Laboratory, (1962).

90. Duggan, J. L., Am. J. Phys., 33, 312 (1965).

91. Ajzenberg-Selove, F., and Lauritsen, T., Nuclear Physics, 11, 139 (1959).

92. McGruer, J. N., Warburton, E. K., and Bender, R. S., Phys. Rev., 100, 235 (1955).

93. Rotblat, J., Phys. Rev., 83, 1271 (1951).

APPENDIX

DETERMINATION OF THE MOMENTUM TRANSFERRED TO THE TARGET NUCLEUS BY THE STRIPPED PARTICLE FOR A $^{11}B(^{3}He,p)^{13}C$ REACTION

The momentum transferred to the target nucleus by the stripped particle is given by Newns (13) as

$$K' = K_3' - \left(\frac{M_{11}}{M_{13}}\right) K_p' \quad , \tag{1}$$

where the primes refer to the center-of-mass coordinate system. From the law of cosines

$$K'^2 = K_3'^2 + \left(\frac{M_{11}}{M_{13}}\right)^2 (K_p')^2 - 2K_3' K_p' \left(\frac{M_{11}}{M_{13}}\right) \text{Cos } \theta \quad , \tag{2}$$

where θ is the scattering angle. The momentum and velocity of the ^{3}He particle in the center-of-mass system are given by

$$\hbar K_3' = M_3 V_3' \tag{3}$$

and

$$V_3' = V_3 - V' \quad , \tag{4}$$

where V_3 is the velocity of the ^{3}He particle in the laboratory system, and V' is the velocity of the center of mass. The kinetic energy of the ^{3}He particle in the laboratory system is given by

$$1/2MV_3^2 = E_3 \quad . \tag{5}$$

The velocity of the center of mass is

$$V' = \left(\frac{M_3}{M_3 + M_{11}}\right) V_3 \quad . \tag{6}$$

Substituting Equation (6) into Equation (4) gives

$$V_3' = \left(\frac{M_{11}}{M_3 + M_{11}}\right) V_3 \quad . \tag{7}$$

Thus, by knowing the incident kinetic energy of the ^{3}He particle, V_3' from Equation (7) and K_3' from Equation (3) can be calculated.

The momentum and kinetic energy of the emitted proton in the center-of-mass system are given by

$$\hbar K_p' = M_p V_p' \quad , \tag{8}$$

and

$$E_p' = 1/2\ M_p (V_p')^2 \quad . \tag{9}$$

The kinetic energy of the two particles before the collision in the center-of-mass system is

$$E_i' = E_3' + E_{11}' \quad , \tag{10}$$

where

$$E_3' = 1/2 M_3 (V_3')^2 = \left(\frac{M_{11}}{M_3 + M_{11}}\right)^2 E_3 \tag{11}$$

and

$$E_{11}' = 1/2 M_{11} (V_{11}')^2 = \frac{M_3 M_{11}}{(M_3 + M_{11})^2} E_3 \quad . \tag{12}$$

Substituting Equations (11) and (12) into Equation (10) gives

$$E_i' = \left(\frac{M_{11}}{M_3 + M_{11}}\right) E_3 \quad . \tag{13}$$

The kinetic energy after the collision is

$$E_f' = E_p' + E_{13}' , \tag{14}$$

where

$$E_p' = 1/2M_p(V_p')^2 \tag{15}$$

is the kinetic energy of the emitted proton and

$$E_{13}' = 1/2M_{13}(V_{13}')^2 \tag{16}$$

is the kinetic energy of the residual nucleus. From the conservation of energy, the kinetic energy associated with the target and projectile can be written as

$$E_i' = E_f' - Q \ . \tag{17}$$

Substituting Equation (13) into Equation (17) gives

$$E_f' = Q + E_3 \left[1 - \frac{M_3}{M_3 + M_{11}} \right] , \tag{18}$$

where E_f' is the kinetic energy after the collision. Using Equation (14), Equation (18) can be written as

$$E_p' + E_{13}' = Q + E_3 \left[1 - \frac{M_3}{M_3 + M_{11}} \right] . \tag{19}$$

The kinetic energy of the residual nucleus is

$$E_{13}' = 1/2M_{13}(V_{13}')^2 = \frac{M_p}{M_{13}} E_p' \ . \tag{20}$$

Substituting Equation (20) into Equation (19) gives the following expression for E_p':

$$E_p' = \left(\frac{M_{13}}{M_p + M_{13}} \right) [E_i' + Q] \ . \tag{21}$$

Once E_p' is known, K_p' is calculated using Equations (8) and (9). After calculating K_3' from Equation (3) for a given kinetic energy of the ^3He particle and K_p' from Equation (8) for the kinetic energy of the emitted proton, Equation (2) can then be used to calculate the momentum transferred to the residual nucleus by the stripped particle.

VITA

The author was born October 13, 1938, in Haralson, Georgia, the second son of Truman and Odus Adair. He received his primary education in the public schools of Paulding County, Georgia, graduating from Dallas High School in May 1956.

By virtue of a Lowry scholarship, he entered Oglethorpe University in September 1956. While at Oglethorpe, he pursued a course of study in Physics and was awarded a degree of Bachelor of Science in June 1960. During his senior year, he was chosen Who's Who in American Colleges and Universities. He was a member of Blue Key, Boar's Head, and LeConte Honorary Societies.

After graduation he was employed by the Union Carbide Corporation at Oak Ridge National Laboratory, Oak Ridge, Tennessee. In September 1961 he enrolled in the graduate program at the University of Tennessee to obtain a Master's Degree in Physics.